Uncertainty Estimation for SMAP Level-1 Brightness Temperature Assimilation at Different Timescales

Alexander Gruber and Rolf H. Reichle

***Abstract*—Soil Moisture Active Passive (SMAP) mission brightness temperature (T_b) observations are assimilated into NASA's Catchment Land Surface Model using an ensemble Kalman filter to update simulations of surface and root-zone soil moisture. Different time-series components of the T_b observations are assimilated, including anomalies, interannual variations, and high-frequency variations. To optimize the weights that the data assimilation (DA) puts on the observations, the ratio between the uncertainties of modeled and observed T_b is approximated using modeled and observed soil moisture uncertainties estimated using triple collocation analysis. In a benchmark experiment, T_b observations are assimilated using a spatially constant 4-K observation uncertainty, as in the operational SMAP Level-4 algorithm. All the DA experiments exhibit notable skill improvements in most regions. Improvements are largest for the interannual variations in the simulations of both surface and root-zone soil moisture (mean improvements in terms of Pearson correlation (–) are 0.08 and 0.06, respectively). Anomaly simulations improve similarly (0.07), and improvements in the high-frequency variations are only observed for surface soil moisture simulations (0.06). No notable difference in skill—neither improvement nor deterioration—is observed between the experiments that use optimized observation uncertainty parameters and the 4-K benchmark experiment. This may be explained by the presence of large observation operator errors, which are analytically shown to have the potential to render postupdate uncertainty insensitive to inaccuracies in estimates of the Kalman gain. These results have important implications for the design of soil moisture DA systems, in particular for parameterizing model and observation uncertainties.**

***Index Terms*—Data assimilation, microwave remote sensing, soil moisture, soil moisture active passive (SMAP).**

I. Introduction

SOIL moisture is an essential climate variable. Knowledge about its dynamics on a global scale is vital for many applications, from agricultural drought monitoring [1] to the study of land–atmosphere interactions [2]. Updating soil moisture states in numerical models by assimilating spaceborne microwave observations has proven useful in a variety of studies and can be done in one of two ways: either by assimilating Level-2 (L2) soil moisture estimates retrieved from the satellite observations, i.e., updating the modeled soil moisture state directly [3], [4], [5], [6], or by assimilating Level-1 (L1) backscatter (σ_0, active microwave) or brightness temperature (T_b, passive microwave) measurements, i.e., using an observation operator to convert model simulations into predictions of σ_0 or T_b, updating these predictions in the observation space, and propagating the updates back into the model's prognostic space through the inverse operation operator [7], [8], [9], [10].

Comparison studies between L1 and L2 data assimilation (DA) generally find very similar performance [7], [11], [12]. It has also been shown analytically that L1 and L2 DA can be equivalent under certain conditions [13], [14]. Therefore, both L1 and L2 DA schemes are being routinely used for operational soil moisture analysis [15], [16]. Nevertheless, L1 DA has some theoretical advantages. For example, many retrieval algorithms require ancillary data (such as vegetation climatologies, soil texture, and land cover information), and it is desirable that these ancillary data are consistent with those used by the model into which the retrievals are assimilated [14], [17], [18], [19]. Also, L1 DA can potentially exploit the entirety of information about land surface variables that is contained in the assimilated radiance measurements by distributing state updates among model predictions of these variables (provided that they are also simulated by the model) [17], [20].

Most relevant for the present study is the consideration of how to best parameterize a Kalman filter (KF) that is used for state updating. The parameters that need to be specified in KF-based systems are the model and observation uncertainties, which determine the amount by which model simulations are corrected [21], [22]. The relative fraction by which model simulations are "pulled toward the observations" is referred to as Kalman gain and depends solely on the *ratio* between model and observation uncertainties, so an optimal functioning of the system (i.e., the maximum possible model uncertainty reduction) can be attained only if this ratio is parameterized accurately [23], [24].

L1 DA systems require the parameterization of uncertainties in radiance space (e.g., T_b), whereas L2 DA systems require the same in retrieval space (e.g., soil moisture). L1 T_b and σ^0 observation uncertainties are fairly well known from calibration activities in the laboratory (during instrument construction) and calibration against stable targets such as the deep sky or Antarctic snowfields (during operation), and they are relatively stable

Manuscript received 1 July 2022; revised 30 September 2022; accepted 17 October 2022. Date of publication 20 October 2022; date of current version 1 November 2022. This work was supported in part by TU Wien Bibliothek through its Open Access Funding Program and in part by the Research Foundation Flanders under Grant FWO-1224320N and Grant FWO-1530019N. The work of Rolf H. Reichle was supported by the NASA Soil Moisture Active Passive mission. *(Corresponding author: Alexander Gruber.)*

Alexander Gruber is with the Department of Geodesy and Geoinformation, Vienna University of Technology, 1040 Vienna, Austria (e-mail: alexander.gruber@geo.tuwien.ac.at).

Rolf H. Reichle is with the Global Modeling and Assimilation Office, NASA Goddard Space Flight Center, Greenbelt, MD 20771 USA (e-mail: rolf.reichle@nasa.gov).

Digital Object Identifier 10.1109/JSTARS.2022.3216213

in both time and space [25], [26]. Crucially, however, in an L1 DA system, the "optimal" weight that ought to be put on L1 observations depends not only on the instrument noise but also on uncertainties in the observation operator that is used to convert between model prognostic space and observation space [10], [11], [14], [27]. That is, in both L1 and L2 DA systems, the "observation uncertainty" (from which to compute the Kalman gain) always comprises both instrument error and observation operator or retrieval algorithm error [14]. The latter component, commonly referred to as representativeness error, contains the totality of all errors other than instrument noise and includes errors due to different representations of spatial and temporal scale as well as errors due to different representations of reality in the model and the observations [28].

A host of strategies to parameterize uncertainties in DA systems have been proposed. The so-called adaptive DA approaches aim to estimate observation and forecast error covariances during the analysis based on internal DA diagnostics, most commonly utilizing the statistical properties of the innovations, i.e., the observation-minus-forecast residuals [21], [22], [29], [30], [31], [32]. For a comprehensive review of innovation-based adaptive DA techniques, we refer the reader to [33]. Crow and Reichle [34] further provide an overview of adaptive methods for land surface DA in particular and tested various approaches for soil moisture updating. A general pattern that seems to emerge for adaptive DA techniques is that methods that work best in reducing forecast uncertainty seem to exhibit excessively slow convergence rates [28], [33], [34], [35], often to a degree where they become computationally infeasible. Sufficiently cost-efficient adaptive methods, in contrast, seem to be incapable of estimating uncertainties accurately enough, probably due to inappropriate assumptions made in their implementation [33], [36], [37]. Owing to the difficulty in estimating forecast and observation uncertainty parameters accurately "online," many studies instead provide the DA system with calibrated uncertainty parameters that are constant in time and/or space [7], [38], [39], [40], which has been shown to yield robust, albeit not "optimal," model simulation improvements.

One way of obtaining such static uncertainty parameters "offline" is to leverage uncertainty estimates from external sources that are independent of the internal functioning of the system [28]. Triple collocation analysis (TCA) [41] is one such approach that has been applied for the assimilation of soil moisture retrievals. For example, Gruber et al. [4], Crow and Van den Berg [37], Gruber et al. [42], and Wu et al. [43] have successfully used TCA-based uncertainty estimates of simulated and observed soil moisture to parameterize different KF-based DA systems. An important limitation of this approach, however, is that TCA has, so far, only been applied to retrievals of biogeophysical variables [44] but not to remotely sensed L1 T_b or σ^0 data. This is because TCA requires three input datasets of the same variable with mutually uncorrelated errors, which are, at present, not available (globally) from currently available sources.

In this study, we propose a hybrid strategy that parameterizes the KF of an L1 T_b DA system with uncertainties estimated from TCA in L2 soil moisture space. The key premise of this approach is that the *ratio* between soil moisture forecast and observation uncertainties estimated from TCA is a reasonably accurate approximation for the *ratio* between T_b forecast and observation uncertainties, even if their absolute magnitudes are very different. Since the Kalman gain is determined exclusively by this uncertainty ratio, such a hybrid approach could allow us to harness L2 retrievals to attain a close-to-optimal functioning of the filter while retaining all the potential benefits of an L1 DA system that were discussed earlier. Our approach implicitly attributes uncertainties in the soil moisture retrieval algorithm to the T_b observations and, as a consequence, also accounts for representativeness error in the observation operator [14], [28]. This is, of course, only true to the degree to which representativeness errors of the retrieval algorithm (from which uncertainties are estimated) are comparable to those of the observation operator (which is used to assimilate T_b observations).

One caveat of the proposed TCA-based approach is that it estimates only spatial patterns of uncertainty, which represent, at each location, the average uncertainty during the whole sample period. While we can anticipate that uncertainties are, in reality, nonstationary [45], [46], it may still be important progress from the both spatially and temporally averaged uncertainty parameters that are used most commonly.

An important related issue that limits the performance of many state-of-the-art soil moisture DA systems is that errors in satellite and model time series have been found to be nonwhite. That is, they exhibit different error variance at different frequencies. This has been demonstrated unequivocally by Draper and Reichle [47], who found that updating soil moisture in a KF-based land DA system using L2 satellite soil moisture retrievals yields varying levels of improvement at different timescales. In their study, updating modeled soil moisture with satellite retrievals resulted in almost twice as large an improvement in unbiased mean squared errors for predictions of interannual soil moisture variations as for predictions of the mean seasonal cycle or short-term soil moisture variations. This suggests that different frequency components of the modeled and observed signals are affected by different sources of uncertainty. In the soil moisture forecasts of a land surface model, for example, low-frequency (LF) errors might result from unmodeled processes such as irrigation [48], whereas high-frequency (HF) errors may stem from errors in transient atmospheric forcing events [47]. In the satellite retrievals, on the other hand, LF errors may stem from an insufficient separation of the soil moisture and the vegetation signal [49], whereas HF error might be dominated by sensor noise [50].

Most state-of-the-art soil moisture DA systems do not account for this frequency dependence of model and observation error. Instead, they parameterize model and observation uncertainties using lumped estimates for the entire frequency spectrum. Using such lumped estimates can only ever be a tradeoff in the degree of uncertainty reduction that the DA can achieve. Even in the best case, it will either be a balance that does not improve either of the frequency components by as much as it potentially could or improve one component as much as possible at the expense of the other. For example, if a satellite product captures interannual variations well but is very noisy in its HF variations,

assimilating that product with the focus on optimizing the interannual variations in the model will inevitably ingest the HF noise as well and could, hence, deteriorate predictions of short-term soil moisture changes.

In this study, we aim to account for this timescale dependence of model and observation uncertainty by estimating uncertainties at different timescales using the TCA-based approach described above. We then investigate whether an EnKF-based DA system that assimilates different frequency components separately using timescale-dependent uncertainty parameters can outperform one that assimilates a lumped anomaly signal using lumped uncertainty parameters, which is the current state of the art.

Section II first summarizes all datasets that are used in this study and describes how they are preprocessed for our experiments. Section III describes the land surface DA setup used in this study, how we assimilate different frequency components of the T_b observations, and how we optimize the uncertainty parameters for the state updating. Section IV summarizes our evaluation strategy. Results are shown in Section V. Finally, Section VI concludes this article.

II. Datasets and Preprocessing

The following datasets were used in this study:

1) meteorological forcing data from NASA's Modern-Era Retrospective analysis for Research and Applications, Version 2 (MERRA-2; DOIs: 10.5067/RCMZA6TL70BG and 10.5067/L0T5GEG1NYFA; available at https://disc.gsfc.nasa.gov/datasets?project=MERRA-2) [51];
2) T_b observations from NASA's Soil Moisture Active Passive (SMAP) mission (L1C Radiometer Half-Orbit 36 km EASE-Grid Brightness Temperatures, Version 5, DOI: 10.5067/JJ5FL7FRLKJI; available at https://nsidc.org/data/spl1ctb/versions/5) [52];
3) passive-microwave-based surface soil moisture retrievals from SMAP (L2 Radiometer Half-Orbit 36 km EASE-Grid Soil Moisture, Version 5, DOI: 10.5067/SODMLCE6LGLL; available at https://nsidc.org/data/spl2smp/versions/5) [53];
4) active-microwave-based surface soil moisture retrievals from the Advanced Scatterometer (ASCAT) onboard the MetOp-A, -B, and -C missions (12.5-km Discrete Global Grid H SAF soil moisture DR H115 and EXT H116, DOI: 10.15770/EUM_SAF_H_0006; available at https://hsaf.meteoam.it/Products/Detail?prod=DATAREC) [54], [55];
5) surface and root-zone soil moisture measurements from the Soil Climate Analysis Network (SCAN) and the U.S. Climate Reference Network (USCRN), drawn from the International Soil Moisture Network (ISMN; available at https://ismn.earth) [56], [57], [58], [59]

For all the analyses (both assimilation and evaluation), data points with a simulated snow mass >0 kg or soil temperature <4 °C are masked out in all datasets. Only SCAN and USCRN measurements that are flagged as "Good" by the ISMN internal quality control [58] are used. ASCAT retrievals, which are derived from $\sim$25 km observations and sampled onto a 12.5-km grid using a 36-km-diameter hamming window, are matched to the 36-km Equal Area Scalable Earth (EASE) Version 2 modeling grid [60] using a nearest-neighbor approach. Datasets are collocated in time using a nearest-neighbor approach and SMAP retrieval times as the reference, allowing a maximum distance of 12 h.

III. Experiment Setup

Our experiment setup is illustrated in Fig. 1 and detailed in the following subsections.

A. DA Setup

SMAP Level-1C T_b observations are assimilated into NASA's Catchment Land Surface Model (CLSM) [61] using the Goddard Earth Observing System land data assimilation system version 17.9.4 (available at https://github.com/GEOS-ESM/GEOSldas/). CLSM land surface simulations are forced with atmospheric simulations from MERRA-2. Model simulations are made over the Contiguous United States (CONUS) on the 36-km EASE v2 grid in 7.5-min intervals and aggregated to 3-h time averages. This assures a maximum time difference of 1.5 h between the model simulations and the assimilated satellite observations. The assimilation period is from April 2015 until March 2021. T_b observations of both ascending and descending orbits, each acquired at both horizontal and vertical polarization, are assimilated using a spatially distributed (3-D) ensemble Kalman filter (EnKF) with 24 ensemble members [39]. A horizontal observation error correlation length of 0.25° and a localization support radius of 1.25° is assumed [11]. A zero-order $\tau-\omega$ model is used as the observation operator to convert model soil moisture and temperature predictions into T_b space, which has been calibrated following the approach of [62].

The EnKF sequentially performs model forecasts and filter updates, also referred to as filter analyses. At each analysis time step, i.e., whenever an observation is available, the EnKF updates the model forecasts as

$$\mathbf{x}_{t,i}^{+} = \mathbf{x}_{t,i}^{-} + \mathbf{K}_t \left(\mathbf{y}_{t,i} - \mathbf{H}\mathbf{x}_{t,i}^{-} \right) \tag{1}$$

where $\mathbf{y}_{t,i}$ is the perturbed observation vector, and $\mathbf{x}_{t,i}^{-}$ and $\mathbf{x}_{t,i}^{+}$ are the perturbed model forecast and analysis state vectors of ensemble member i at time step t, respectively. The EnKF state vector consists of CLSM prognostic variables for soil moisture (surface excess and root-zone excess), surface (skin) temperature, and surface soil heat content as in the operational SMAP Level-4 (L4) product [63]. Note that, for the evaluation of our DA experiments, surface (0–10 cm) and root-zone (0–100 cm) soil moisture estimates are diagnosed from these prognostic soil moisture variables. The observation operator $\mathbf{H}$ converts prognostic state variables into T_b predictions at both horizontal and vertical polarization. The $\tau-\omega$ model used here as the operation operator is actually nonlinear, but to aid presentation and without loss of generality, we use a linear operator $\mathbf{H}$ in the equations shown here. $\mathbf{K}_t$ denotes the Kalman gain, which is calculated as

$$\mathbf{K}_t = \mathbf{P}_t^{-}\mathbf{H}_t^{\intercal} \left(\mathbf{H}_t \mathbf{P}_t^{-} \mathbf{H}_t^{\intercal} + \mathbf{R}_t \right)^{-1} \tag{2}$$

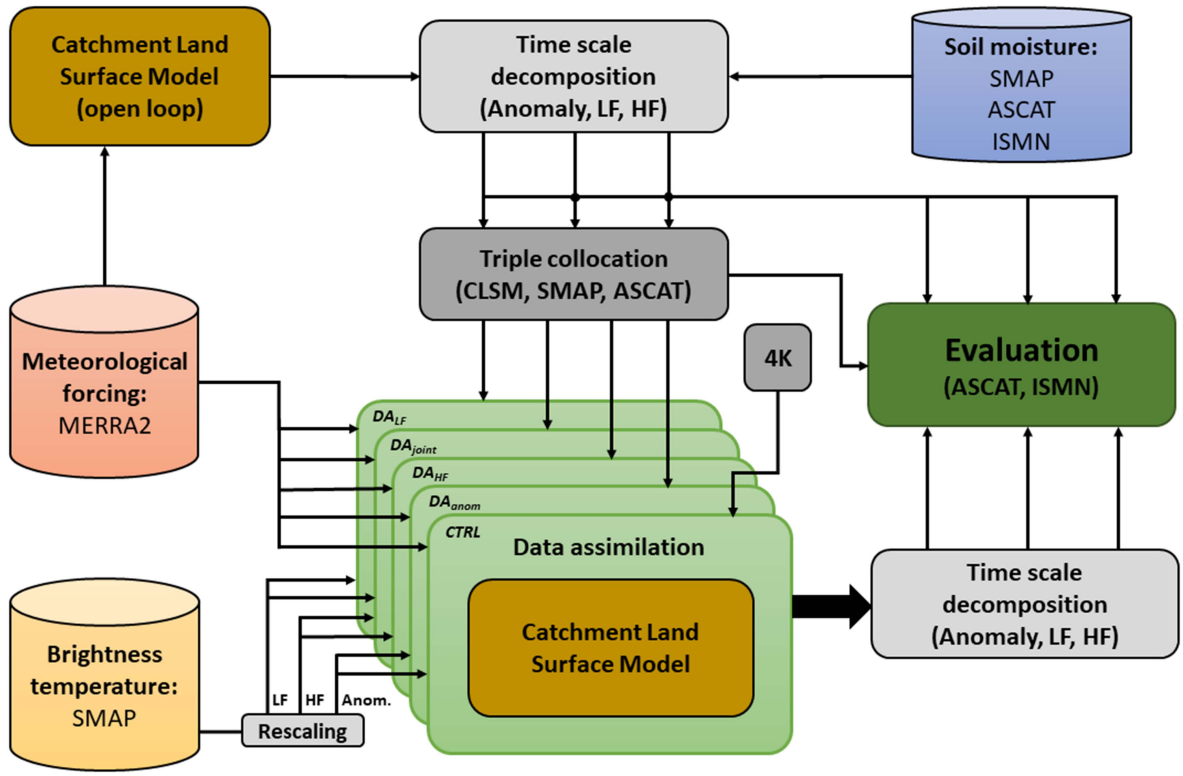

Fig. 1. Illustration of the experiment setup. TCA is applied to SMAP, CLSM, and ASCAT soil moisture. Uncertainties are estimated separately for anomalies, the LF signal, and the HF signal. These uncertainty estimates are used to optimize the Kalman gain for assimilating either anomalies (DA_{anom}), the LF signal (DA_{LF}), or the HF signal (DA_{HF}) alone or for jointly assimilating both the LF and the HF signal (DA_{joint}). The $CTRL$ experiment that serves as a benchmark uses a constant observation error standard deviation of 4 K. The skill of the DA experiments is evaluated on the same timescales using both ASCAT retrievals and ISMN measurements. TCA uncertainty estimates for ASCAT are used to mitigate the influence of ASCAT uncertainties on relative skill evaluation metrics.

where $\mathbf{P}_t^-$ is the forecast error covariance matrix that is diagnosed from the model ensemble and includes both the propagated analysis error and the model perturbation that is added at each time step, and $\mathbf{R}_t$ is the observation error covariance matrix that is diagnosed from the observation ensemble. Note that by exploiting simulated (ensemble-based) error correlations between the surface and root-zone excess reservoirs, the analysis also includes updates to the modeled root-zone soil moisture [39].

B. Assimilation at Different Timescales

The KF is "bias-blind" [64]. That is, systematic biases between model forecasts and satellite observations can substantially deteriorate DA performance. In such bias-blind systems, systematic differences are thus typically removed by rescaling the observations into the model space before assimilation [11], [65], [66]. This is most commonly done by removing differences between the model and observation climatology and causes the system to assimilate so-called (climatological) anomalies, which are the residuals from the mean seasonal cycle [67], [68], [69], [70].

However, as demonstrated by Draper and Reichle [47], it might be useful to break these anomalies down into two distinct signal components at different frequencies: 1) interannual variations, which represent LF deviations from the climatic pattern such as prolonged drought in a given year (hereinafter referred to as the LF signal); and 2) HF variations that represent short-term weather-driven soil moisture changes, e.g., due to individual precipitation events (hereinafter referred to as the HF signal). The different signal components are illustrated in Fig. 2 for an example T_b model time series at a random location in our study domain. Since these components are influenced by different sources of error, assimilating them as separate signals allows us to optimize the KF for their frequency-specific uncertainty (see Section III-E). In this study, we test four ways of assimilating the different frequency components of T_b observations:

1) assimilating anomalies, i.e., the lumped HF plus LF signals [see Fig. 2(b)], as it is commonly done;
2) assimilating the LF signals alone [Fig. 2(c), green];
3) assimilating the HF signals alone [Fig. 2(c), gold];
4) jointly assimilating the LF and HF components as separate signals with separate uncertainty estimates [Fig. 2(c), gold, green].

The different frequency components are estimated following [71], separately for the model estimates and the observations. First, a 35-day moving-average filter is applied to the T_b time series. The HF signal component [see Fig. 2(c), gold] is then calculated by subtracting this moving-average time series from the raw T_b time series. Next, a seasonally varying T_b climatology [see Fig. 2(a), blue] is derived by averaging the moving-average T_b time series for each calendar day across all years of the study period. The anomalies [see Fig. 2(b)] are then estimated by subtracting this mean seasonal cycle from the raw T_b time series. Finally, the LF signal component [see Fig. 2(c), green]

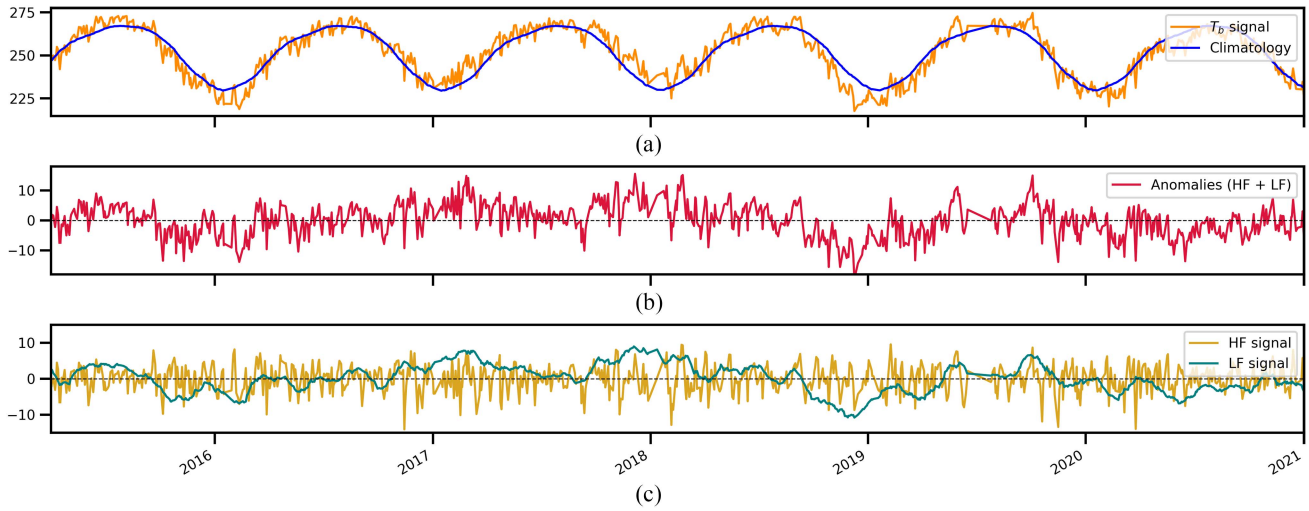

Fig. 2. Illustration of the most relevant frequency components in a T_b time series (in Kelvin). (a) Raw T_b time series and its mean seasonal cycle, i.e., the climatology. (b) Anomalies, i.e., residuals from the climatology. (c) Separate LF and HF components contained in the anomalies.

is estimated by subtracting the HF signal from the anomaly time series. The same approach is used to estimate anomalies, LF signals, and HF signals for soil moisture time series (see Section III-E1). Note that the use of 35-day window filters limits the application of the proposed approach in near real-time applications to a minimum of 17.5-day latency.

C. Observation Rescaling

The T_b observations are rescaled prior to assimilation following the approach of [16]. This rescaling causes the DA innovations to retain only the bias-corrected differences between the modeled and observed signal components that are assimilated. More specifically, observations are rescaled by subtracting the differences between those components of the observed and modeled signals that are *not* assimilated. That is, to assimilate anomalies, the differences between the observed and simulated T_b climatologies are subtracted from the T_b observations; to assimilate the LF signal, differences between observed and simulated T_b climatologies as well as HF variations are subtracted from the T_b observations; and to assimilate the HF signal, differences between observed and simulated T_b climatologies as well as LF variations are subtracted from the T_b observations.

D. Experiment Summary

The DA experiments that we run are summarized in Table I. In the experiments labeled DA$_*$, we test the various ways of assimilating different T_b frequency components described above. In each of these experiments, the EnKF is optimized for the uncertainties of the assimilated frequency components using the approach described in the following subsection. The $CTRL$ experiment serves as a benchmark and assimilates anomalies using a constant value of 4 K for the observation error standard deviation in the entire study domain, as it is done in the generation of the operational SMAP L4 product [39], [63]. These 4 K comprise $\sim$1.3 K instrument error and $\sim$3.8 K representativeness error. For all the experiments, we use the CLSM model perturbation settings and model parameters (boundary conditions) of the SMAP L4_SM Version 4 product. Note, however, that we run our model simulations at a 36-km spatial resolution instead of a 9-km resolution.

TABLE I
EXPERIMENT OVERVIEW

Exp. name	Assim. freq. component	T_b obs. error variance
$CTRL$	HF + LF (anomalies)	4^2 K^2
DA_{anom}	HF + LF (anomalies)	tuned using s.m. $\mathbf{P}/\mathbf{R}$
DA_{LF}	LF	tuned using s.m. $\mathbf{P}/\mathbf{R}$
DA_{HF}	HF	tuned using s.m. $\mathbf{P}/\mathbf{R}$
DA_{joint}	HF, LF (jointly)	tuned using s.m. $\mathbf{P}/\mathbf{R}$ (separately for LF and HF)

The term "s.m. P/R" refers to the soil moisture uncertainty ratio (see Section III-E).

E. KF Optimization

As mentioned, the optimal functioning of a KF-based DA system requires the correct parameterization of the *ratio* between the forecast and observation error covariance matrices ($\mathbf{P}_t$ and $\mathbf{R}_t$), which determines the Kalman gain [see (2)]. For simplicity, we will refer to this ratio hereinafter as the $\mathbf{P}$-to-$\mathbf{R}$ ratio, or $\mathbf{P}/\mathbf{R}$, for short. In this study, we propose to approximate $\mathbf{P}/\mathbf{R}$ in L1 T_b space—as required by our L1 DA system—with $\mathbf{P}/\mathbf{R}$ values estimated from model forecasts and observations in L2 soil moisture space. To optimize our system for the different DA experiments described above (see Table I), $\mathbf{P}/\mathbf{R}$ values are estimated separately for each assimilated signal component (i.e., LF variations, HF variations, and anomalies, which comprise both LF and HF variations; see Section III-B and Fig. 2).

1) Soil Moisture Uncertainty Estimation: Soil moisture uncertainties are estimated by applying TCA [41], [72] to CLSM "open-loop" (OL, i.e., model-only) ensemble simulations without DA and L2 surface soil moisture retrievals from SMAP and ASCAT. TCA provides estimates for the "true" random error variances of three datasets, that is, uncertainty estimates for

one dataset do not depend on which other datasets are chosen to complete the triplet. This requires a set of assumptions to be met, most importantly that the errors of the three datasets are independent of one another [44]. The triplet used here is commonly assumed to meet these assumptions [71]. TCA estimates random error variances $\widehat{\mathrm{var}}(\varepsilon_{\Theta,i})$ (where Θ, i refers to soil moisture estimates of dataset i, and ε to their associated random errors) for CLSM OL surface soil moisture simulations and SMAP surface soil moisture retrievals as

$$\begin{aligned}\widehat{\mathrm{var}}(\varepsilon_{\Theta,\mathrm{clsm}}) &= \mathrm{var}(\Theta_{\mathrm{clsm}}) \\ &\quad - \frac{\mathrm{cov}(\Theta_{\mathrm{clsm}},\Theta_{\mathrm{ascat}})\,\mathrm{cov}(\Theta_{\mathrm{clsm}},\Theta_{\mathrm{smap}})}{\mathrm{cov}(\Theta_{\mathrm{ascat}},\Theta_{\mathrm{smap}})} \\ \widehat{\mathrm{var}}(\varepsilon_{\Theta,\mathrm{smap}}) &= \mathrm{var}(\Theta_{\mathrm{smap}}) \\ &\quad - \frac{\mathrm{cov}(\Theta_{\mathrm{smap}},\Theta_{\mathrm{ascat}})\,\mathrm{cov}(\Theta_{\mathrm{smap}},\Theta_{\mathrm{clsm}})}{\mathrm{cov}(\Theta_{\mathrm{ascat}},\Theta_{\mathrm{clsm}})}\end{aligned} \tag{3}$$

where $\mathrm{var}(\cdot)$ and $\mathrm{cov}(\cdot)$ denote the temporal variance and covariance, respectively. Note that $\widehat{\mathrm{var}}(\varepsilon_{\Theta})$ represents time-average uncertainties. Equations in (3) are applied separately to estimate uncertainties of modeled and observed time-series anomalies, LF signal components, and HF signal components. Since TCA estimates are unreliable if not all three datasets are sufficiently related to one another, grid cells where any two of the considered time series in the triplets exhibit a Pearson correlation <0.2 are masked out in all subsequent analyses. The following section describes how we use these TCA-based uncertainty estimates to tune $\mathbf{P}/\mathbf{R}$ for our DA system in T_b space. For more details about TCA, we refer the reader to [44].

2) Filter Parameterization: As mentioned, we aim to use the ratio between TCA-based uncertainty estimates of modeled and observed soil moisture—that is, $\mathbf{P}/\mathbf{R}=\widehat{\mathrm{var}}(\varepsilon_{\Theta,\mathrm{clsm}})/\widehat{\mathrm{var}}(\varepsilon_{\Theta,\mathrm{smap}})$—to parameterize the ratio between the KF uncertainty parameters associated with model simulations and satellite observations of T_b, thus optimizing the Kalman gain. In an EnKF, the forecast and observation error covariance matrices ($\mathbf{P}_t^-$ and $\mathbf{R}_t$) that are used to calculate the Kalman gain are diagnosed from the ensembles, i.e., calculated as the forecast and observation ensemble (co)variances, respectively. Ensemble (co)variances result from assumed model and observation perturbations, i.e., errors that are drawn from assumed probability distributions and added to the model simulations (and their forcing variables) and the observations at each time step. Optimizing $\mathbf{P}_t^-$ and $\mathbf{R}_t$, and hence $\mathbf{P}/\mathbf{R}$, therefore requires changing the perturbation parameters so that the ensemble variances will take on the values we desire for $\mathbf{P}_t^-$ and $\mathbf{R}_t$, respectively.

Adjusting the observation ensemble spread to a target value is straightforward because errors are assumed to be temporally white, zero-mean, and Gaussian distributed. Therefore, choosing a particular value for the perturbation variance causes the observation ensemble to exhibit precisely that variance (within the sampling noise afforded by the finite ensemble size). Tuning the ensemble variance of T_b model simulations, however, is more complicated. This is because realistic variability in the soil moisture and temperature simulations (from which T_b simulations are diagnosed using the observation operator) is typically achieved by perturbing both model forcing variables (to account for forcing data uncertainty) and model soil moisture predictions (to account for model deficiencies). The T_b ensemble spread is, thus, the result of an autocorrelated blend of forcing and (prognostic) state perturbations, and it is virtually impossible to predict *a priori* how exactly this T_b ensemble spread will change when the model perturbation parameters are altered. Therefore, we tune our EnKF toward a desired $\mathbf{P}/\mathbf{R}$ value by keeping $\mathbf{P}$ as it is and changing $\mathbf{R}$ only. Before describing the exact optimization of $\mathbf{R}$ in detail, the following section summarizes the model perturbations that we have used for all experiments.

3) Model Perturbation: Model diagnostic T_b simulations are perturbed indirectly by: 1) perturbing precipitation forcing with a multiplicative log-normal factor (mean of 1 and standard deviation of 0.5); 2) perturbing short-wave radiation forcing with a multiplicative log-normal factor (mean of 1 and standard deviation of 0.3); 3) perturbing long-wave radiation forcing with an additive error (standard deviation of 20 W/m^2); and 4) perturbing the model prognostic catchment deficit and root-zone excess simulations with an additive error (standard deviation of 0.24 and 0.16 kg/m^2/h, respectively). Model forcing perturbations are assigned a spatial and temporal autocorrelation of 0.5° and 24 h, respectively, and model prognostic perturbations of 0.3° and 3 h, respectively. Error cross-correlation is assumed between precipitation and short-wave radiation (-0.8), between precipitation and long-wave radiation (0.5), and between short-wave and long-wave radiation (-0.5). These values have been established by previous studies and are considered to lead to a realistic spread for both soil moisture and T_b ensemble simulations [66]. Keeping them at these established values, thus, likely helps us to maintain a realistic propagation of forecast uncertainty between state updates.

4) Observation Perturbation: To tune $\mathbf{P}/\mathbf{R}$ for our filter toward the uncertainty ratio that we estimate in soil moisture space, T_b observation uncertainties are calculated as follows. First, a time-average model uncertainty $\hat{\mathbf{P}}$ is diagnosed from the CLSM OL T_b ensemble variances that result from the model perturbations described above:

$$\hat{\mathbf{P}} = \left\langle \mathrm{var}\left(\mathbf{H}\mathbf{x}^-\right)\right\rangle. \tag{4}$$

The Gaussian brackets $\langle\cdot\rangle$ denote the temporal average; here, $\mathrm{var}(\cdot)$ denotes the ensemble variance. An optimized value $\hat{\mathbf{R}}_{\mathrm{opt}}$ for the observation uncertainty is then obtained as

$$\hat{\mathbf{R}}_{\mathrm{opt}} = \hat{\mathbf{P}}\,\frac{\widehat{\mathrm{var}}(\varepsilon_{\Theta,\mathrm{smap}})}{\widehat{\mathrm{var}}(\varepsilon_{\Theta,\mathrm{clsm}})}. \tag{5}$$

This optimized observation uncertainty $\hat{\mathbf{R}}_{\mathrm{opt}}$ is estimated at each grid cell for each frequency component that we consider in the different experiments described above (see Section III-D, Table I). It is worth emphasizing that the (spatial) tuning of $\mathbf{P}/\mathbf{R}$ is not intended to account for (spatial) variations in T_b measurement error, which is known precisely and fairly stable in both space and time [26], but predominantly for variations due to representativeness error in the observation operator [14].

F. Caveats

A few caveats of the proposed $\mathbf{P}/\mathbf{R}$ tuning approach need to be discussed.

1) Our TCA-based estimates represent temporal averages of model and observation uncertainty. Equation (5), thus, provides only a single, time-invariant estimate for the observation uncertainty, which will lead to a stationary observation ensemble variance. Model background uncertainty ($\mathbf{P}_t^-$), however, is evolving and generally reduced whenever observations are assimilated. This will likely cause the Kalman gain to be underestimated in some instances and overestimated in others.
2) Kalman gains are optimized for the performance of the observations relative to *OL* model simulations. Since the assimilation should progressively reduce model background uncertainty throughout the assimilation period, our optimized Kalman gains will likely be systematically overestimated.
3) The observation operator that we use (a zero-order $\tau - \omega$ model) is nonlinear. Consequently, the optimal value for the Kalman gain depends on the state of the prognostic variables themselves. Using temporally constant observation uncertainties will, thus, inherently lead to suboptimal filtering performance. Note, however, that this issue affects not only the uncertainty tuning approach proposed here in particular but also any DA system that uses static observation uncertainties together with a nonlinear state-variable-dependent observation operator.
4) For the L1 T_b DA system, $\mathbf{P}/\mathbf{R}$ is tuned using soil moisture uncertainties estimated from L2 soil moisture retrievals through TCA. Representativeness errors of the L2 retrieval algorithm are, thus, used as a proxy for representativeness error in the observation operator of our L1 DA system. For TCA, we use the official SMAP L2 soil moisture product, which employs a retrieval algorithm (including ancillary data) that is similar, but not identical, to the radiative transfer model that constitutes our observation operator. Therefore, $\mathbf{P}/\mathbf{R}$ may be either over- or underestimated, depending on whether the official SMAP L2 retrieval algorithm is more or less accurate than our observation operator.
5) Uncertainty in model simulations of soil temperature also leads to uncertainty in simulations of T_b. These temperature-induced uncertainties are not accounted for in our TCA-based proxy estimates for P, which are derived from just soil moisture estimates. At the same time, TCA-based uncertainty estimates for SMAP soil moisture retrievals implicitly account for potential soil temperature input uncertainties in the retrieval algorithm. Taken together, this will cause the DA system to put too little weight on the observations when using TCA-based estimates for tuning $\mathbf{P}/\mathbf{R}$.
6) TCA provides us with a single estimate for the uncertainty of modeled and observed soil moisture, yet we assimilate SMAP T_b observations from both ascending and descending orbits, acquired at both H and V polarization, all of which are likely to exhibit slightly different uncertainties. Even though we apply (5) separately for all these observation types to estimate the observation uncertainties, these estimates are likely to be slightly inaccurate in each case.

All of these issues can lead to inaccuracies in the Kalman gain and, therefore, adversely impact DA performance. In this study, we test whether their combined effect is small enough so that our proposed observation uncertainty tuning approach leads to a better filtering performance than using a single lumped observation error for the entire assimilation domain as is the current state of the art.

IV. Evaluation Strategy

For all DA experiments (see Table I), we evaluate the skill gain (or loss) relative to OL simulations of the frequency components that are affected by the assimilation and for which they are optimized. That is, for the $CTRL$ and DA_{joint} experiments, we evaluate their skill in predicting each frequency component, including anomalies, LF variations, and HF variations. For the DA_{anom}, DA_{LF}, and DA_{HF} experiments, we evaluate only their skill in predicting anomalies, LF variations, and HF variations, respectively.

A. In Situ Evaluation

DA skill is evaluated directly against 186 and 106 ground reference stations from the SCAN and USCRN networks, respectively, which are distributed homogeneously over the CONUS (see Fig. 3). DA skill is evaluated for both surface (0–10 cm) and root-zone (0–100 cm) soil moisture simulations at different timescales using the Pearson correlation coefficient as a performance metric.

B. ASCAT Evaluation

DA skill over the entire CONUS is further evaluated using ASCAT surface soil moisture retrievals. Ideally, this would be done using TCA. But, since the errors of the DA analyses are correlated with errors in both SMAP soil moisture retrievals and the CLSM OL simulations, we are no longer able to construct a triplet from model and satellite data (with CONUS-wide coverage) that meet the basic assumption of uncorrelated errors. To circumvent this issue, we employ the approach proposed by Gruber et al. [73]: We first evaluate DA skill in terms of the relative Pearson correlation with respect to ASCAT retrievals, which we then correct for the influence of ASCAT uncertainty obtained from TCA applied to ASCAT, SMAP, and CLSM OL soil moisture:

$$\rho_{\text{DA}} = \frac{\rho_{\text{DA,ASCAT}}}{\rho_{\text{ASCAT}}} \tag{6}$$

where $\rho_{i,j}$ denotes the Pearson correlation coefficient and ρ_i denotes the (TCA-based) correlation coefficient w.r.t. the unknown truth [74].

C. DA Diagnostics

Many studies utilize internal DA diagnostics to verify the optimal functioning of their DA systems [16], most commonly

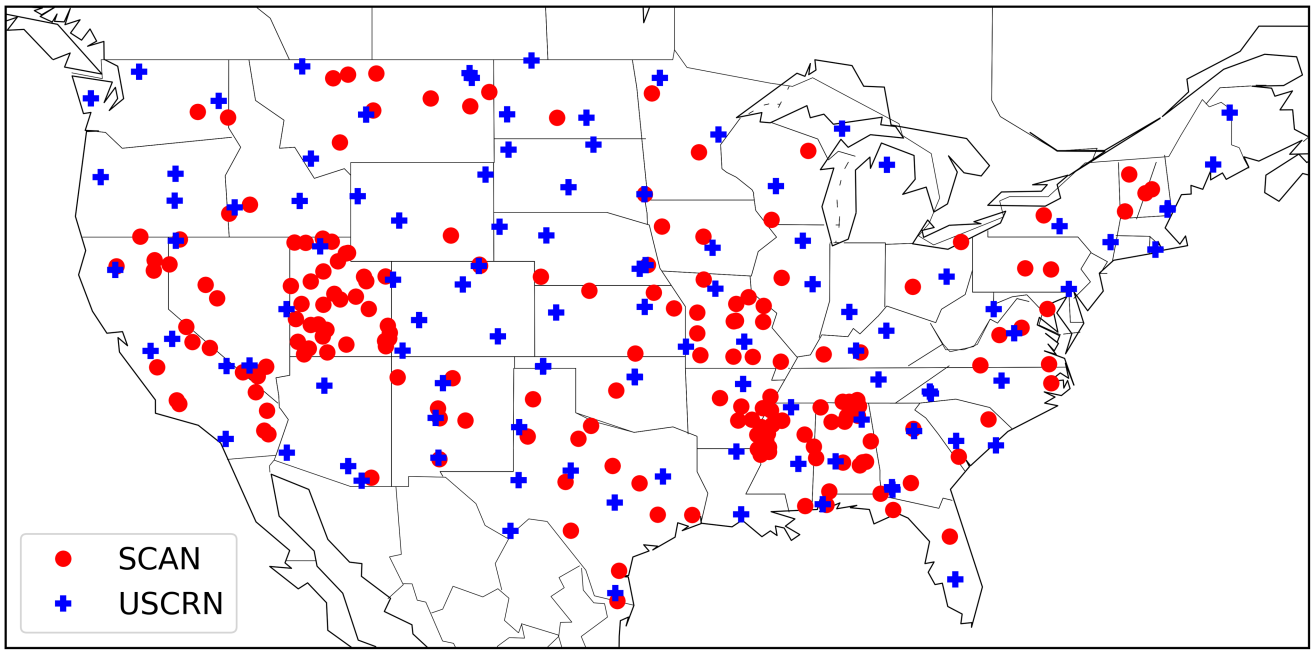

Fig. 3. Locations of the 186 SCAN (red dots) and 106 USCRN (blue crosses) sites that provide valid ground measurements during our study period.

the behavior of the innovations, i.e., the differences between the observations and the pre-update forecasts ($\mathbf{y}_t - \mathbf{H}\mathbf{x}_t^-$). Of particular interest for this study is the temporal innovation autocorrelation (IAC), which holds information about the correct parameterization of $\mathbf{P}/\mathbf{R}$. The IAC indicates whether the KF sufficiently pulls the model predictions toward the observations: if observation uncertainty is overestimated (relative to model uncertainty) and the Kalman gain is too low, the IAC should be positive; if observation uncertainty is underestimated and the Kalman gain is too high, the IAC should be negative; and if $\mathbf{P}/\mathbf{R}$ and, hence, the Kalman gain are parameterized correctly, the IAC should be zero [34]. However, this is true only if errors are not temporally autocorrelated. If they are—and in our case, they are likely to be—the IAC will take on a positive value even if the KF is working optimally [37]. We calculate the IAC (as the lag-1 Pearson correlation in the innovation series) for our DA experiments nonetheless, assuming that a *reduction* in IAC between experiments is still indicative of an improvement in filtering performance.

V. Results and Discussion

A. TCA-Based Uncertainties

Fig. 4 shows the TCA-based estimates for the error standard deviations of the anomalies (a, d), the LF signal component (b, e), and the HF signal component (c, f) of SMAP soil moisture retrievals (a–c) and CLSM OL surface soil moisture simulations (d–f). Notice that in many areas where SMAP exhibits lower or higher uncertainties in the LF signal than in the HF signal, it is the other way around for CLSM simulations. This suggests that the DA system should indeed benefit from assigning different weights to the different frequency components.

HF and LF signal errors can reasonably be assumed to be orthogonal (i.e., mutually uncorrelated) because they are largely caused by different mechanisms (see Section I). Hence, since the anomalies are the sum of the HF and the LF signals, their error variance too should be the sum of the LF and HF error variances. However, some error cross-correlations between the two frequency components may be introduced by the nonorthogonal transformation (i.e., the moving-average based approach described in Section III-B) that we use to decompose the frequencies of the raw time series [47]. To assess whether (or to which degree) this is the case, we calculate the difference between the anomaly error standard deviation and the square root of the sum of the HF and LF error variances $(\widehat{\mathrm{std}}(\varepsilon_{\Theta,\mathrm{anom}}) - (\widehat{\mathrm{var}}(\varepsilon_{\Theta,\mathrm{HF}}) + \widehat{\mathrm{var}}(\varepsilon_{\Theta,\mathrm{LF}}))^{1/2})$. Fig. 5 shows these differences for SMAP and CLSM, respectively. The differences are very small, implying that no noteworthy cross-correlations exist. We can, therefore, confidently assimilate the LF and HF signals together without having to take error cross-correlations into account.

B. Observation Uncertainties

Fig. 6 shows the optimized observation uncertainties ($\hat{\mathbf{R}}_{\mathrm{opt}}$) that are derived for each observation type (orbit direction and polarization) from the TCA-based soil moisture uncertainty estimates for the different timescales (see Fig. 4) using the proposed $\mathbf{P}/\mathbf{R}$ tuning approach [see (5)]. Differences between the uncertainties of ascending and descending orbits appear negligible, whereas H-polarized observations are assigned uncertainties that are larger (by $\sim$0.7 K on average) than those of V-polarized observations. Remember, however, that the observation uncertainties are determined from soil moisture uncertainties that do not distinguish between polarizations. The apparent difference in the uncertainties for H- and V-polarized observations results

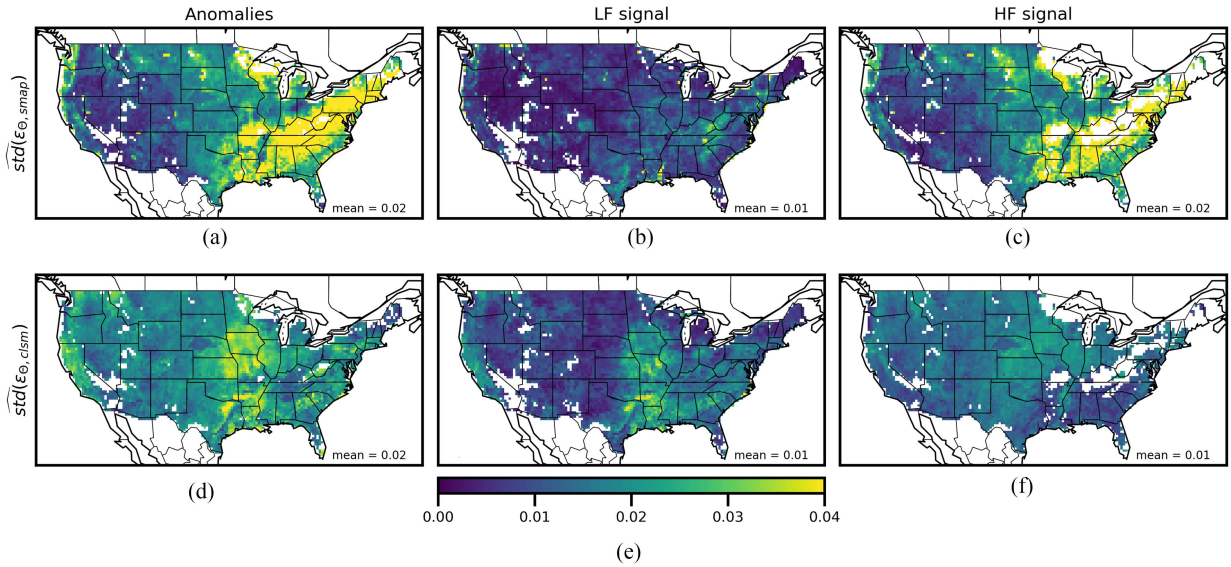

Fig. 4. TCA-based error standard deviation estimates (m^3/m^3) for (a)–(c) SMAP soil moisture retrievals and (d)–(f) CLSM OL soil moisture simulations. Errors are estimated for (a), (d) anomalies, (b), (e) LF soil moisture variations, and (c), (f) HF soil moisture variations. Grid cells with unreliable TCA estimates are masked out (see Section III-E1).

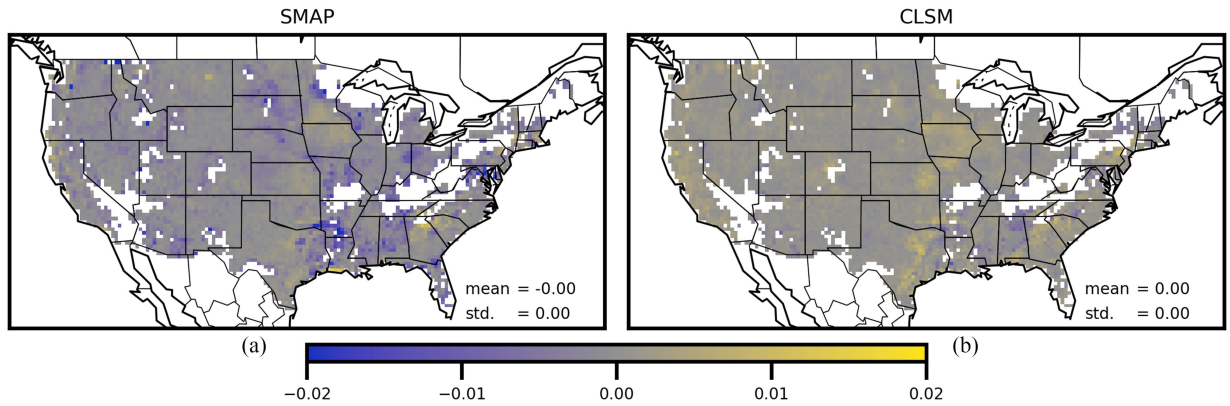

Fig. 5. Differences between the TCA-based error standard deviation estimates (m^3/m^3) of anomalies and the square root of the sum of error standard deviation estimates of the LF and HF signals, for (a) SMAP and (b) CLSM. Grid cells with unreliable TCA estimates in any of the frequency components are masked out (see Section III-E1).

from larger uncertainties in H-polarized model T_b simulations. These are counterbalanced by (5) with larger observation uncertainties that lead to the same $\mathbf{P}/\mathbf{R}$ values for both polarizations. As a result, the Kalman gain is the same for the assimilation of H- and V-polarized observations. As mentioned in Section III-F, not accounting for the polarization dependence of observation uncertainties might adversely impact DA performance.

Apart from the differences between polarizations, clear spatial patterns exist in the observation uncertainties that are distinctly different at each timescale. Uncertainties of the LF signals are generally lower than those of the HF signals, which indicates that larger skill gains can be expected on the LF timescale. This is consistent with what has been observed by Draper and Reichle [47]. Blue colors in Fig. 6 indicate regions where observation uncertainties are lower than the spatially constant 4 K that are used in the $CTRL$ experiment (i.e., more weight is put on them in the assimilation) and yellow colors indicate regions where they are higher (i.e., less weight is put on them in the assimilation). Mind, however, that the spatial observation uncertainty patterns shown in Fig. 6 do not directly reflect the spatial patterns of the observation weights (which will be shown later) because these depend on $\mathbf{P}/\mathbf{R}$, which also accounts for the uncertainty of the model.

To account for possible systematic differences between $\mathbf{P}/\mathbf{R}$ in soil moisture and T_b space, we tested adding synthetic inflation and deflation factors to the T_b uncertainties before assimilation (both additive and multiplicative with varying magnitudes), but the uncertainty values derived initially (see Fig. 6) achieved the best performance in the DA skill evaluations. Results are, therefore, only shown for these experiments.

C. Weight Verification

To verify whether the observation uncertainties $\hat{\mathbf{R}}_{\text{opt}}$ shown in Fig. 6 correctly calibrate $\mathbf{P}/\mathbf{R}$ in T_b space toward the ratio between model and observation uncertainties in soil moisture

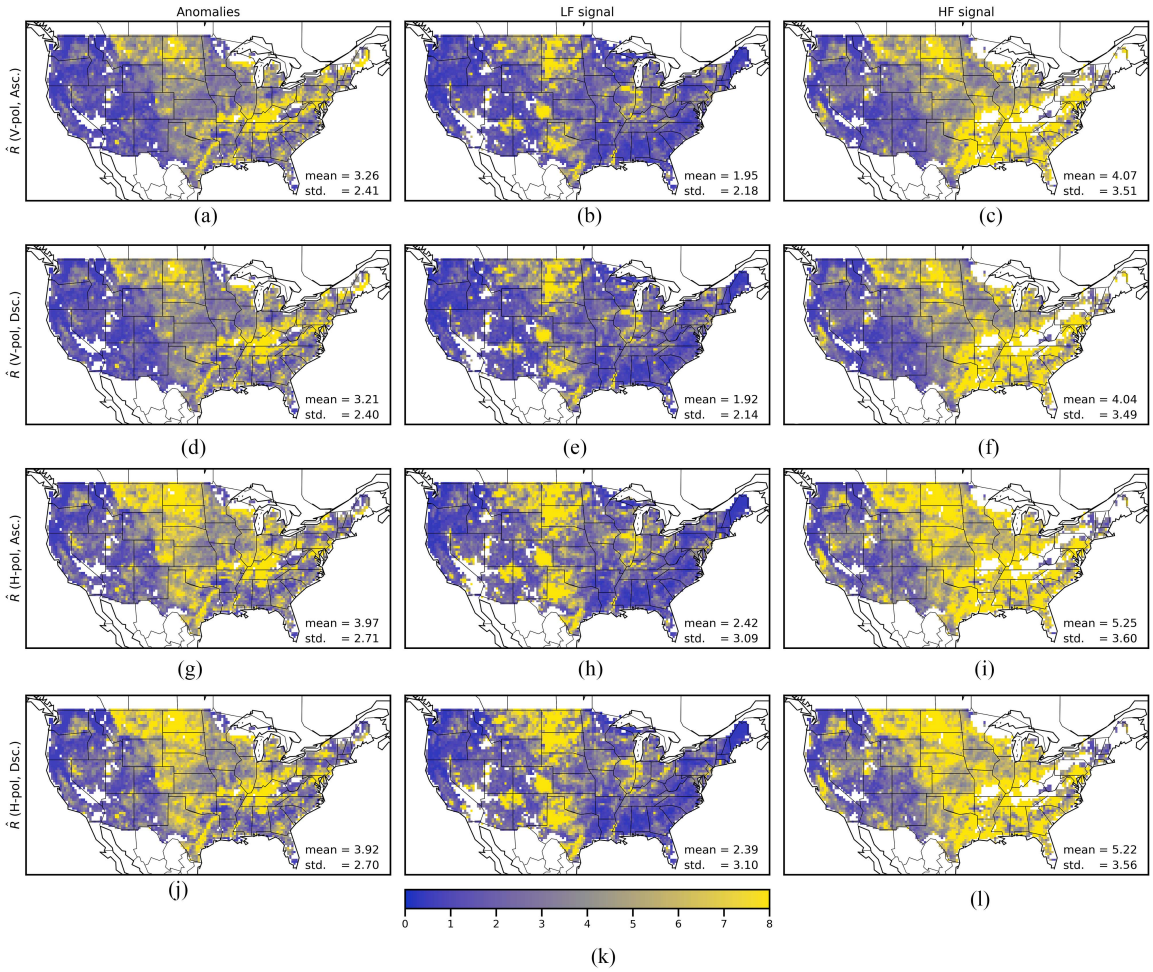

Fig. 6. Standard deviation of the T_b uncertainties (K) used for different observation types (orbit direction and signal polarization; y-axis), optimized for the assimilation of anomalies [DA_{anom}; (a), (d), (g), and (j)], LF T_b variations [DA_{LF} and DA_{joint}; (b), (e), (h), and (k)], and HF T_b variations [DA_{HF} and DA_{joint}; (c), (f), (i), and (l)], respectively. The color scale is centered on the 4 K error standard deviation that is used in the $CTRL$ experiment. Blue (yellow) colors indicate that the optimized DA experiments (DA_*) put more (less) weight on the observations than the $CTRL$ run. Grid cells with unreliable TCA estimates are masked out (see Section III-E1).

space (see Fig. 4), as intended by (5), we diagnose the actual T_b forecast and observation ensemble standard deviations (i.e., $\text{var}(\mathbf{Hx}^-)$ and $\text{var}(\mathbf{y})$) that result from using the estimated $\hat{\mathbf{R}}_{\text{opt}}$ values in an OL model simulation. Fig. 7(a)–(c) shows the TCA-based soil moisture uncertainty ratios at each timescale, and Fig. 7(e)–(g) shows the corresponding ratios between T_b forecast and observation ensemble standard deviations averaged over all time steps and observation types (i.e., orbit direction and polarization). To aid visual interpretation, ratios are linearized by converting them into decibel (dB) units (zero dB means that the ratios are equal to one and every additional ± 3 dB correspond to an additional doubling or halving of the ratio). Yellow colors indicate regions where model simulations have larger errors than the satellite observations (resulting in large weights for the observations) and blue colors indicate areas where it is the other way around (resulting in small weights for the observations). We can see that (5) can reliably estimate observation uncertainties $\hat{\mathbf{R}}_{\text{opt}}$ that lead to a desired T_b ensemble variance and, hence, $\mathbf{P}/\mathbf{R}$.

For comparison, Fig. 7(d) shows the ensemble variance ratio for the $CTRL$ experiment that results when using the constant 4 K observation uncertainty everywhere. The overall $\mathbf{P}/\mathbf{R}$ pattern in the $CTRL$ experiment is similar to that of the tuned P/R patterns in the anomaly and HF frequency components [see Fig. 7(e) and (g)] but differs markedly from the $\mathbf{P}/\mathbf{R}$ pattern of the LF component [see Fig. 7(f)].

Fig. 7 is also a (nonlinear, monotonic) proxy for the spatial distribution of the weights that the KF will put on the observations. On average, the $CTRL$ experiment assigns less weight to the observations than do DA experiments with the tuned $\mathbf{P}/\mathbf{R}$ values (i.e., DA_*), especially in the Western U.S. Clear differences exist between the spatial weight patterns for the different signal components. While the weights estimated for anomalies [see Fig. 7(e)] and the HF signals [see Fig. 7(g)] exhibit very similar patterns—albeit with a generally lower magnitude for the latter—the spatial distribution of weights estimated for the LF signals [see Fig. 7(f)] is distinctively different. Most noticeable, SMAP observation weights for the LF signal remain relatively high over the Eastern U.S., whereas those of the other frequency components are small or close to zero.

Many soil moisture retrieval assimilation studies mask out these areas because increasing vegetation density has been associated with increasing uncertainty in microwave soil moisture

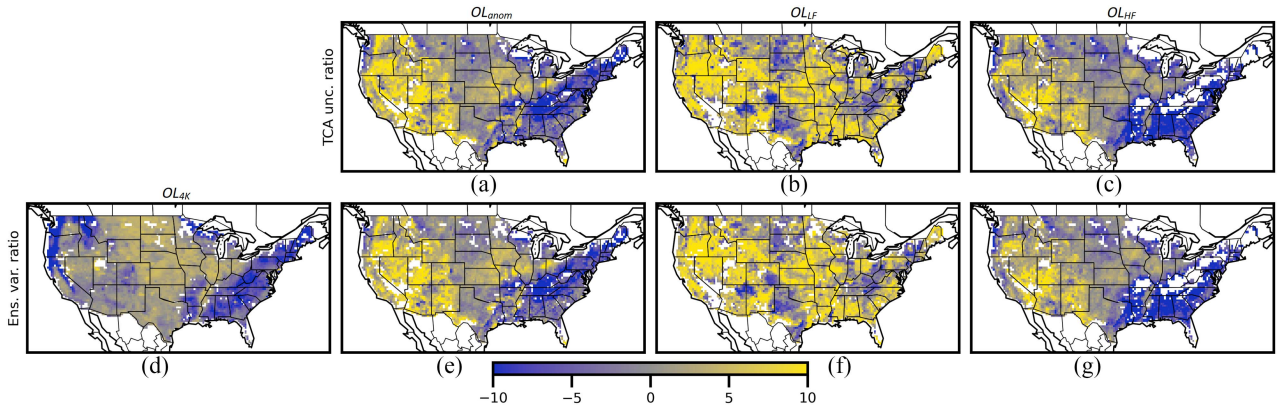

Fig. 7. $\mathbf{P}/\mathbf{R}$ ratios expressed in dB units: between TCA-based soil moisture uncertainty estimates for OL model and observation anomalies (a), LF signal variations (b), and HF signal variations (c); and between (average) OL model and observation T_b ensemble standard deviations when using a constant 4 K observation uncertainty (d) or an observation uncertainty that has been optimized for assimilating anomalies (e), the LF signal component (f), or the HF signal component (g). Yellow (blue) colors indicate that observation uncertainties are smaller (larger) than OL forecast uncertainties. Grid cells with unreliable TCA estimates are masked out (see Section III-E1).

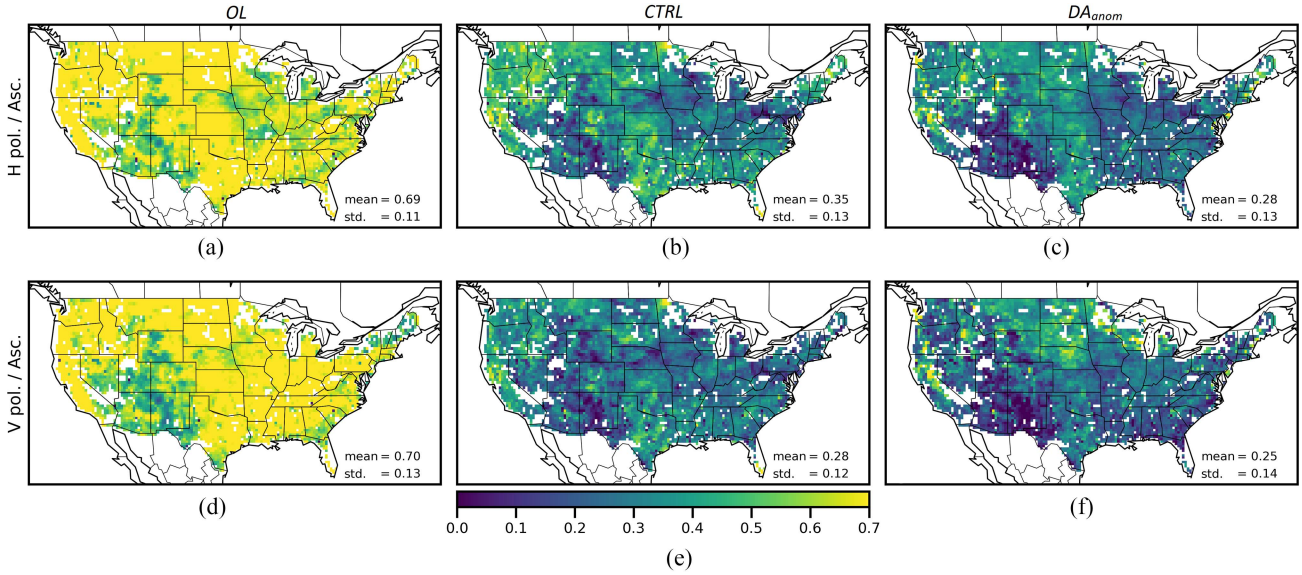

Fig. 8. IAC (–) of H-polarized (a)–(c) and V-polarized (d)–(f) data from ascending orbits for the OL run (a), (d), the $CTRL$ experiment (b), (e), and the DA_{anom} experiment (c), (f), respectively. Grid cells with unreliable TCA estimates are masked out (see Section III-E1).

retrievals [75]. While there might indeed be a point where too dense vegetation attenuates microwave signals to a degree where they are no longer sensitive to soil moisture, this appears to be the case only over tropical rain forests [76]. Notwithstanding, it has been posited that apparent soil moisture information contained in microwave measurements over densely vegetated areas may be a result of the correlation between soil moisture and vegetation water content dynamics [77]. This conjecture is consistent with the fact that our optimization strategy estimates large observation weights only on the LF timescale and does so not as a result of excessively large model error but because of small observation error (see Fig. 4). Whatever the mechanism, it seems that SMAP T_b observations may still contain useful soil moisture information on the LF timescale (i.e., about interannual variations), which will be explored further in Section V-E.

D. Internal Diagnostics

Fig. 8 shows the IAC (see Section IV-C) of both H- and V-polarized T_b for the OL run, the $CTRL$ experiment, and our DA experiment that has been optimized for the assimilation of anomalies (DA_{anom}). We do not show IAC estimates for the other optimized DA runs because DA_{anom} is the only experiment whose innovations can be compared directly to those of the $CTRL$ run. Only IAC estimates for ascending orbits are shown because they are virtually identical to those of descending orbits (as is expected from Fig. 6).

Both DA experiments substantially reduce the IAC compared to the OL run: spatial averages of the IAC for DA_{anom}, $CTRL$, and OL are 0.28, 0.35, and 0.69 for H polarization and 0.25, 0.28, and 0.70 for V polarization, respectively. This indicates a proper functioning of the filter in both DA cases. The fact that

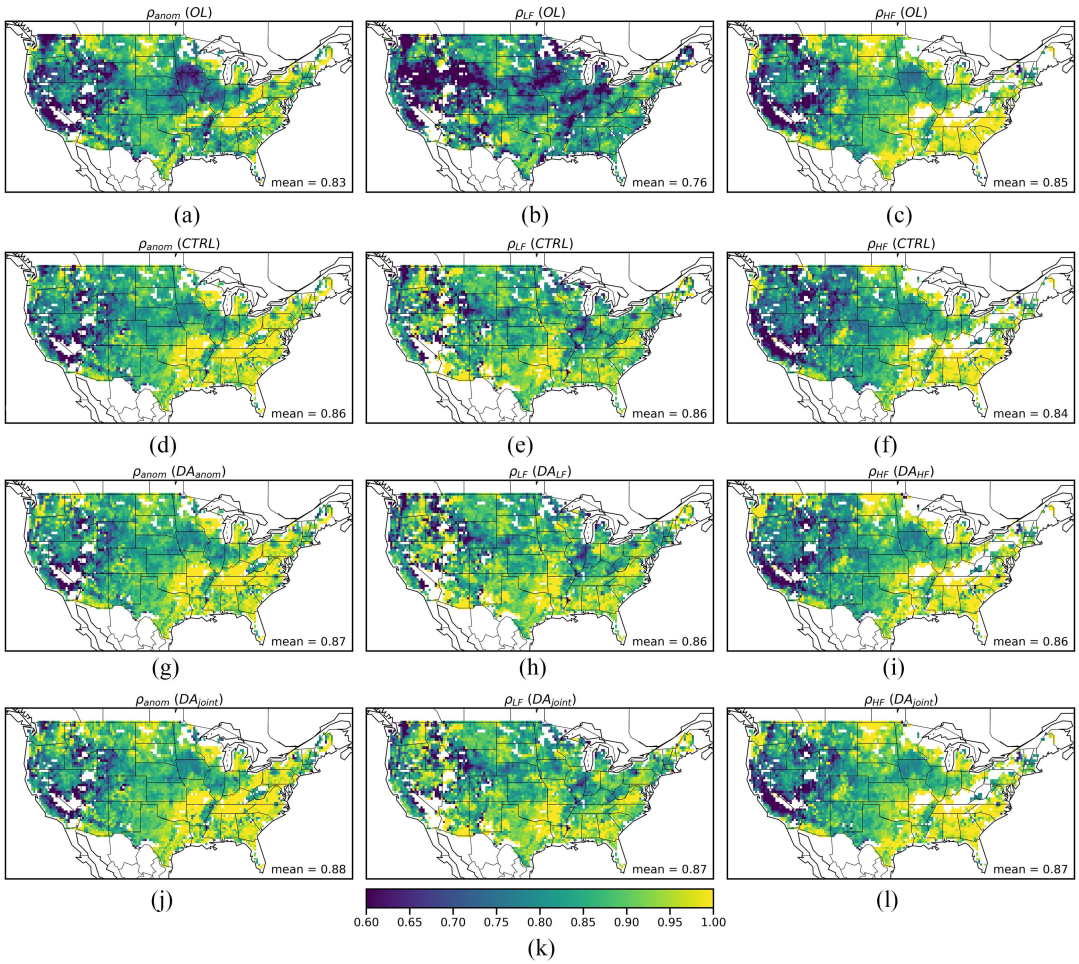

Fig. 9. Skill ρ_* (–) of the OL run [(a)–(c)]; the $CTRL$ experiment [(d)–(f)]; the optimized DA experiments that assimilate either anomalies [DA_{anom}; (g)], LF T_b variations [DA_{LF}; (h)], or HF T_b variations [DA_{HF}; (i)]; and the optimized DA experiment that jointly assimilates both LF and HF T_b variations [DA_{joint}; (j)–(l)]. The skill is shown for estimates of surface soil moisture anomalies [ρ_{anom}; (a), (d), (g), and (j)], LF variations [ρ_{LF}; (b), (e), (h), and (k)], and HF variations [ρ_{HF}; (c), (f), (i), and (l)]. Grid cells with unreliable TCA estimates are masked out (see Section III-E1).

DA_{anom} consistently yields lower IACs than $CTRL$ suggests that our optimized uncertainties are closer to the "truth" than is the constant 4 K uncertainty used in $CTRL$. However, the differences in IAC between DA_{anom} and $CTRL$ are small.

E. Reference Data Comparison

1) ASCAT Evaluation: Fig. 9 shows the skill of the OL run (a–c), the $CTRL$ run (d–f), and the DA_* experiments with optimized observation uncertainty parameters (g–l). "Skill" refers to the Pearson correlation of the anomalies (ρ_{anom}), LF variations (ρ_{LF}), and HF variations (ρ_{HF}) with respect to ASCAT, corrected for the uncertainty in ASCAT observations [see (6)]. Fig. 10 further shows the relative skill differences between the optimized DA_* experiments and the OL run (a–f) and between the optimized DA_* experiments and the $CTRL$ run (g–l). Blue colors represent areas where the optimized DA_* experiments perform better than the OL simulations or the $CTRL$ run, and red colors represent areas where they perform worse.

Overall, assimilating SMAP T_b observations yields large skill improvements in the LF component of the soil moisture predictions [see Fig. 10(b) and (e)]. Improvements in predicting soil moisture anomalies [see Fig. 10(a) and (d)] are about half that of the LF skill gains, and average skill differences are negligible for predicting HF soil moisture variations [see Fig. 10(c) and (f)]. This is, of course, only true for the experiments that actually assimilate the respective signal components. The lack of improvements in the HF signal component might be explained by the fact that our land surface model applies a rain gauge correction to the meteorological forcing, and that the gauge coverage over our study domain (the CONUS) is substantial. It is, therefore, not unexpected that the assimilation of satellite observations does not add additional information about individual rainfall events. Much larger skill improvements in the HF component upon assimilation can be expected in regions with poor rain gauge coverage such as most developing countries [78], [79].

Using optimized observation uncertainties leads to consistently larger skill gains than are obtained with the 4 K observation uncertainty used in the $CTRL$ experiment [see Fig. 10(g)–(l)]. However, differences in skill between the optimized DA_* and $CTRL$ experiments are very small, if not negligible, except

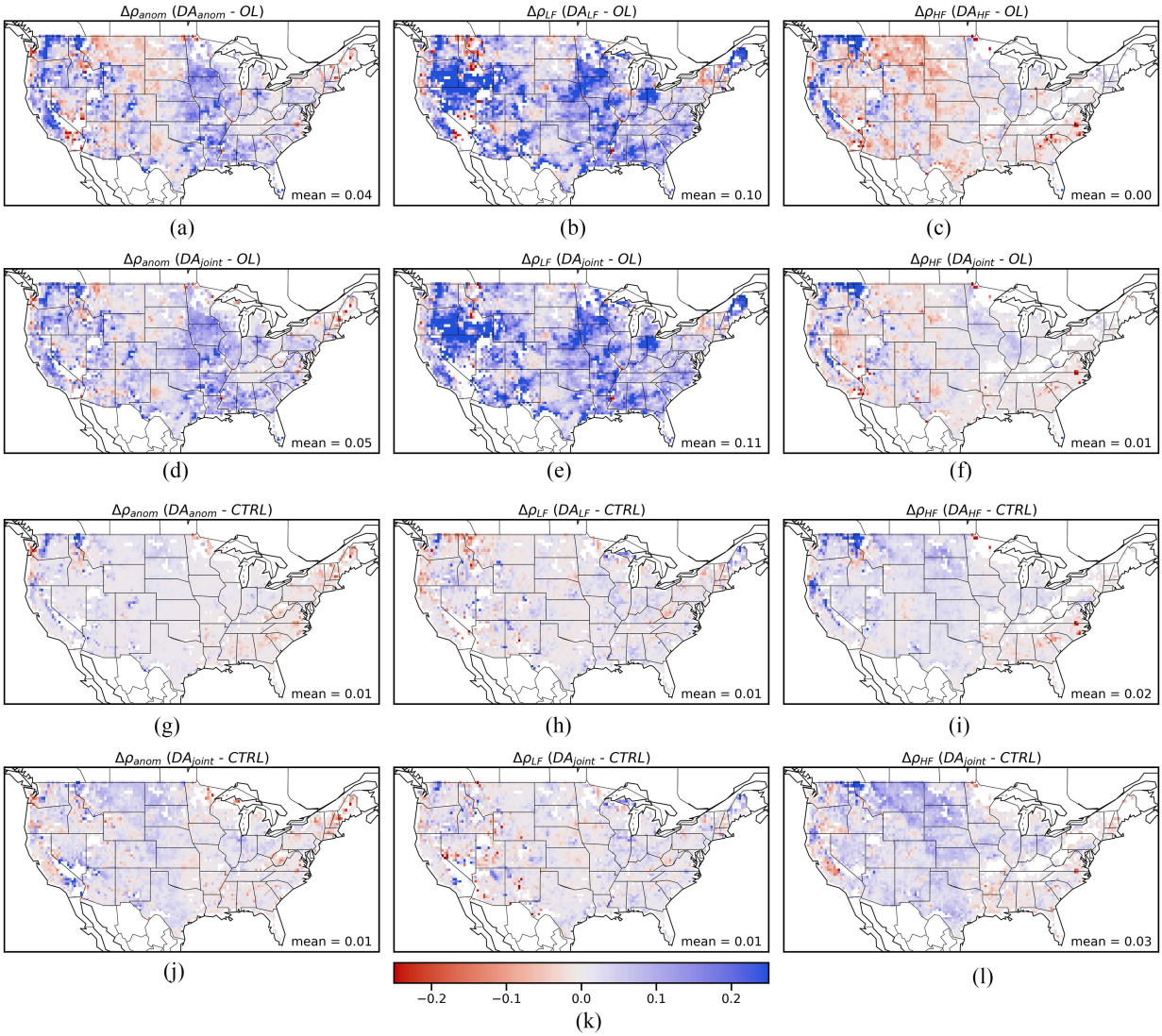

Fig. 10. Skill differences $\Delta\rho_*$ (–) between the optimized DA_* experiments and the OL run [(a)–(f)] and between the optimized DA_* experiments and the $CTRL$ run [(g)–(l)]. Skill differences are shown for estimates of surface soil moisture anomalies [$\Delta\rho_{\text{anom}}$; (a), (d), (g), and (j)], LF variations [$\Delta\rho_{\text{LF}}$; (b), (e), (h), and (k)], and HF variations [$\Delta\rho_{\text{HF}}$; (c), (f), (i), and (l)]. Grid cells with unreliable TCA estimates are masked out (see Section III-E1).

for predictions in the HF signal component, and then only when jointly assimilating both the LF and the HF part of the signal [see Fig. 10(l)]. In this case, DA_{joint} performs consistently (albeit only slightly) better than the $CTRL$ run. The fact that additionally assimilating the LF signal benefits HF soil moisture predictions hints at some residual error cross-correlations between the two.

Irrigated areas such as the Corn Belt or the Mississippi river region stand out as regions with large skill improvements over the OL simulations (predominantly for the LF signal and anomalies, but to a smaller degree also for HF variations). This is true for both our optimized DA_* experiments and the $CTRL$ run, and it is in line with studies that suggest that satellite observations hold valuable information about anthropogenically driven soil moisture changes that are not accounted for in CLSM (or in other common models) [48], [80]. Particularly noteworthy is that we see large skill improvements, especially for predicting LF signal variations, in the more densely vegetated areas of the Southeast of our domain. As mentioned earlier, these regions are often masked out in soil moisture retrieval assimilation studies because microwave signals are presumed to be insensitive to soil moisture in these regions, but our results suggest that SMAP observations indeed contain valuable information about interannual soil moisture variability even over dense vegetation. Nevertheless, this information can only be leveraged fully when assimilating—and weighting—the LF signal separately. This is because assigning a similarly large weight to the HF component of the observations—which are much more uncertain (see Fig. 4)—substantially deteriorates the performance of HF model simulations upon assimilation (not shown).

More generally, areas of notable skill gain coincide well with areas with large $\mathbf{P}/\mathbf{R}$ values (i.e., areas where CLSM OL skill is significantly lower than that of SMAP; see Fig. 7). Even though large skill gains can only be expected where the T_b observations are given large weights, the fact that these anticipated skill improvements are indeed realized indirectly validates our tuned

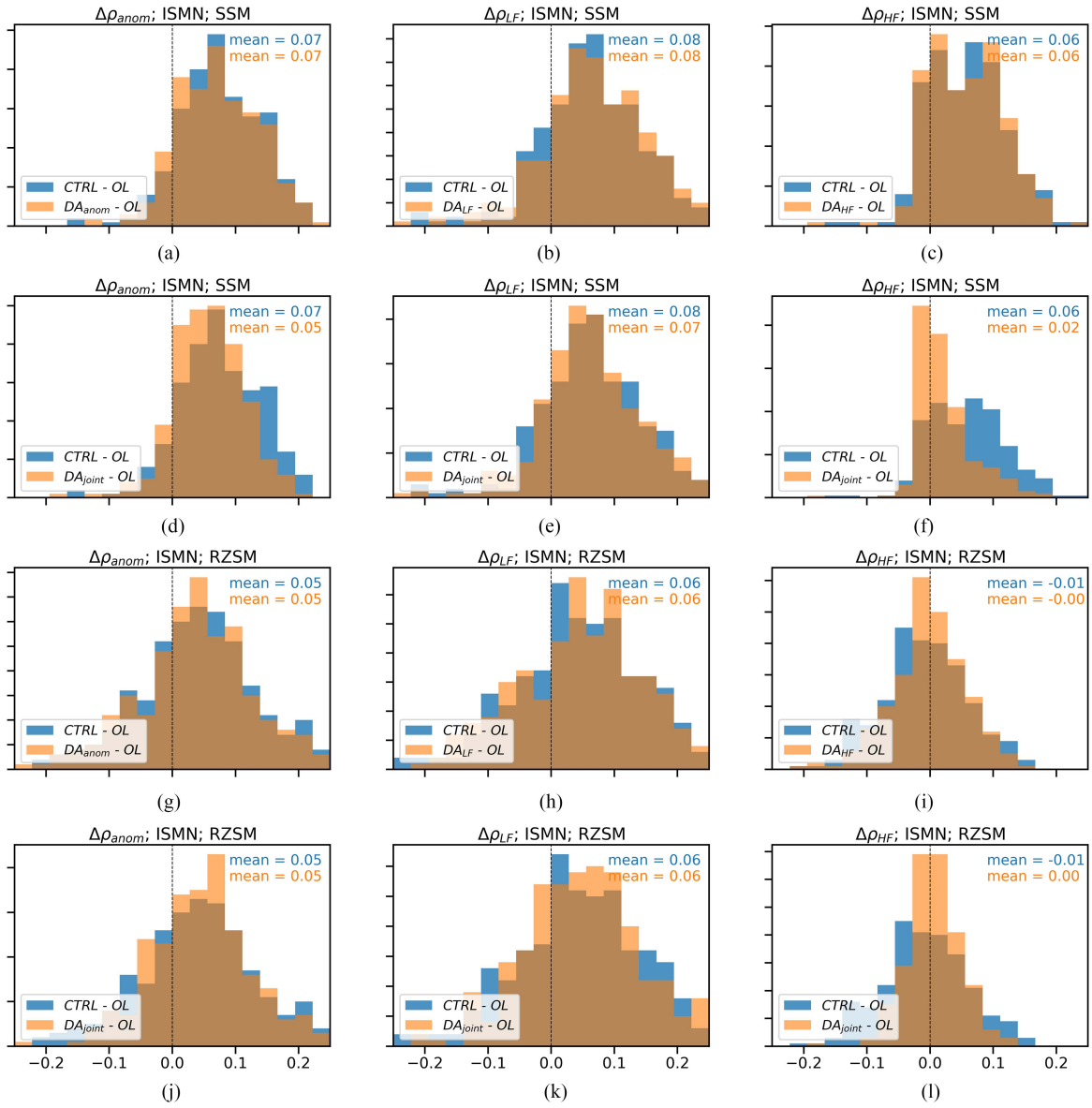

Fig. 11. Histograms of the DA skill differences $\Delta\rho_*$ (–) between the $CTRL$ experiment and the OL run (blue) and between the optimized DA_* experiments and the OL run (orange). "Skill" refers to the correlation against surface soil moisture [SSM; (a)–(f)] and root-zone soil moisture [RZSM; (g)–(l)] ground measurements from the $ISMN$. Histograms are shown for predictions of anomalies [$\Delta\rho_{\text{anom}}$; (a), (d), (g), and (j)], the LF signal component [$\Delta\rho_{\text{LF}}$; (b), (e), (h), and (k)], and the HF signal component [$\Delta\rho_{\text{HF}}$; (c), (f), (i), and (l)].

uncertainty estimates. This is because if the tuned observation uncertainties were underestimated, assimilating the observations would deteriorate model performance instead of benefiting it, and if observation uncertainties were overestimated, we would not see large skill improvements in the first place. On the other hand, the fact that the skill remains virtually unchanged when using optimized observation uncertainties versus using a constant value of 4 K everywhere, even though there are substantial differences between them (see Fig. 6), suggests that our EnKF system is actually insensitive to the parameterization of model and observation uncertainties. This will be further explored analytically in Section V-F.

2) In Situ Evaluation: Fig. 11 shows histograms of the DA skill improvement (or degradation) with respect to the OL skill for the $CTRL$ (blue) and DA_* (orange) experiments at the SCAN and USCRN locations (see Fig. 3). "Skill" refers to the correlation against surface soil moisture [SSM; Fig. 11(a)–(f)] and root-zone soil moisture [RZSM; Fig. 11(g)–(l)] ground measurements. For comparison, Fig. 12 shows the histograms of the correlations against SSM retrievals of ASCAT (instead of ground measurements) for the same experiments over the same locations. Note that histograms of the correlations against ASCAT are virtually identical when calculated over the whole study region rather than over the site locations only (not shown). The skill assessments against the in situ measurements can thus, in turn, be considered representative for the entire domain.

Results are largely consistent with the ASCAT-based evaluation shown earlier. DA generally improves model performance compared to the OL run (both in the optimized DA_* experiments and in the $CTRL$ run). This is true for both surface and root-zone

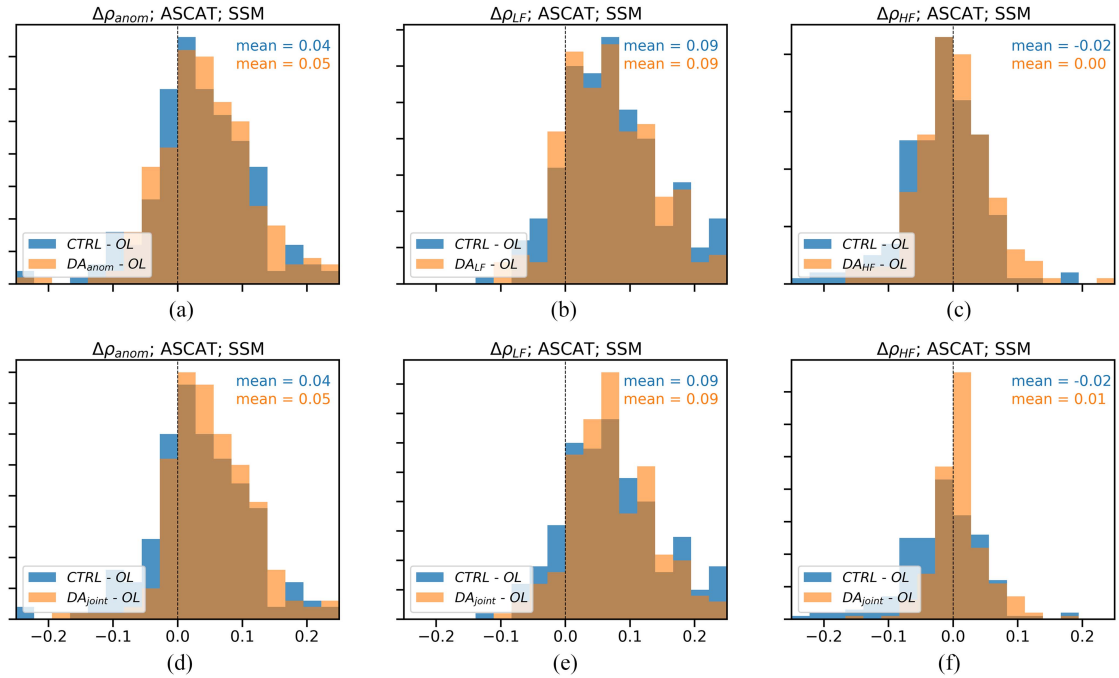

Fig. 12. As in Fig. 11(a)–(f), but for skill differences $\Delta\rho_*$ calculated against surface soil moisture retrievals from ASCAT instead of ISMN ground measurements. Histograms are calculated over the same ISMN site locations as Fig. 11(a)–(f).

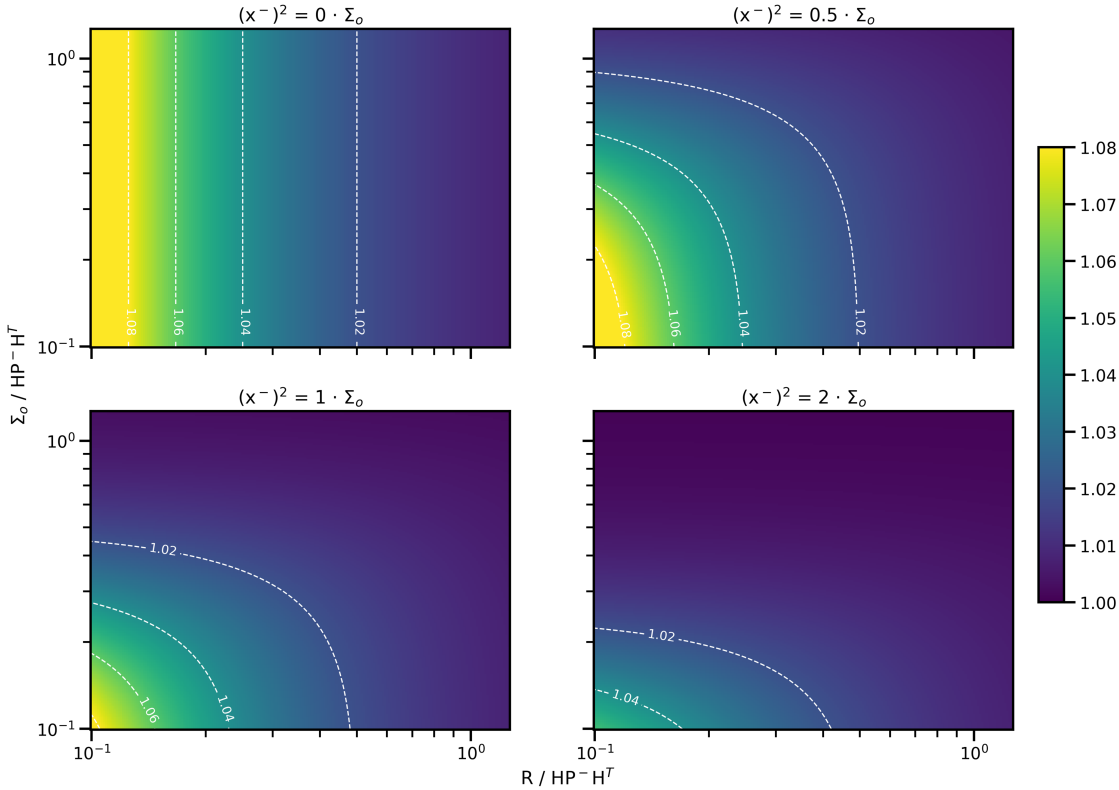

Fig. 13. Fractional change in the postupdate uncertainty P^+ (–) that results from a 10% deviation from the optimal Kalman gain as a function of: 1) the observation error relative to model forecast error (x-axis); 2) the representativeness error relative to model forecast error (y-axis); and 3) the magnitude of the model state. The latter is shown for states being 0 (top left), 0.5 (top right), 1 (bottom left), and 2 (bottom right) times the representativeness error standard deviation.

soil moisture. Skill improvements in the LF signal component [see Fig. 11(b), (e), (h), and (k)] are larger than for anomalies [see Fig. 11(a), (d), (g), and (j)], although this is less evident in the in situ evaluation (where the skill of the anomalies improves almost as much as that of the LF variations) than it is in the evaluation against ASCAT [see Fig. 12(b), (e) and (a), (d)]. While the DA does not seem to benefit HF soil moisture predictions when evaluated against ASCAT [see Figs. 10 and 12(c) and (f)], correlations of the HF signal against in situ measurements do indeed improve notably, albeit only for surface soil moisture predictions [see Fig. 11(c) and (f)]. HF signal improvements in root-zone soil moisture predictions are not expected, however, because root-zone soil moisture does not vary rapidly. The fact that HF soil moisture predictions improve when evaluated against in situ data but not when evaluated against ASCAT suggests that SMAP may be able to capture precipitation events that are not accurately retrieved by ASCAT (possibly due to its generally lower signal-to-noise ratio) nor properly modeled in the CLSM. However, it may also be that ASCAT is simply not a well-suited reference to evaluate improvements in the HF soil moisture predictions because of its temporal misalignment with SMAP observations and coinciding or shortly preceding precipitation events.

Improvements in ρ_{anom}, ρ_{LF}, and ρ_{HF} are slightly larger in the DA_{anom}, DA_{LF}, and DA_{HF} experiments, respectively, than they are in the DA_{joint} experiment. This is particularly true for ρ_{HF} and hints at residual error cross-correlations in the LF and HF signal components. These most likely result from the nonorthogonal transformation used to decompose the signal into different frequencies (see Section III-B). Nevertheless, consistent with the CONUS-wide evaluation is the fact that the optimized observation uncertainties—especially for DA_{anom}, DA_{LF}, and DA_{HF}—do not appear to yield better or worse outcomes than using a constant 4 K observation error. This, again, suggests that our EnKF system is not very sensitive to the parameterization of the model and observation uncertainties, which is perhaps the most striking result of our study. Earlier studies that compared different uncertainty optimization approaches have reported similar findings [81], yet the reason for this behavior remained elusive.

F. Skill Gain Dependence on Representativeness Error

A plausible explanation for the apparent lack of sensitivity of DA skill to the observation uncertainty parameterization might lie in the common oversimplification of representativeness error. It has been long known that representativeness error (i.e., error in the observation operator) is state variable-dependent [14], yet most studies—including the one presented here—treat it as a state-invariant term that can simply be added to measurement error [28]. Doing so, however, could cause the representativeness error to limit the amount of observational information that *can* be gleaned from assimilating L1 observations, regardless of how well model and measurement uncertainties are parameterized. In this section, we attempt to demonstrate this by analytical means. A complete analytical account on the influence of representativeness error for the complex DA system employed here is beyond the scope of this article, but substituting a simple derivation of the main idea assuming linearity may provide helpful insights [28].

Let us, therefore, revisit the KF update equation and the definition of the associated Kalman gain [see (1) and (2)] considering a scalar case with a linear observation operator

$$x^+ = x^- + K\left(y - Hx^-\right) \tag{7}$$

where x^- and x^+ are the (scalar) forecast and the analysis, respectively, H is the (linear) observation operator, and K is the Kalman gain. The analysis uncertainty follows from the law of the propagation of uncertainties as

$$P^+ = \left(\frac{\partial x^+}{\partial x^-}\right)^2 P^- + \left(\frac{\partial x^+}{\partial y}\right)^2 R + \left(\frac{\partial x^+}{\partial H}\right)^2 \Sigma_o$$

$$= (1 - HK)^2 P^- + K^2 R + K^2 x^{-2} \Sigma_o \tag{8}$$

where P^- and P^+ are the forecast and analysis error variance, respectively, and Σ_o is the operation operator error variance (i.e., the representativeness error). In the standard derivation of the KF equations, Σ_o is neglected (or approximated simply by inflating R) and (8) takes on the well-known form of $P^+ = (1 - HK)P^-$. The optimal observation weight (i.e., Kalman gain) is obtained by setting the derivative of the analysis uncertainty with respect to the Kalman gain to zero ($\frac{\partial P^+}{\partial K} = 0$) and then solving for the Kalman gain, which yields

$$K = \frac{HP^-}{H^2 P^- + R + x^{-2}\Sigma_o}. \tag{9}$$

Equation (9) differs from the standard definition of the Kalman gain [see (2)] by the additional third term in the denominator ($x^{-2}\Sigma_o$), which is state variable dependent. As mentioned, this state variable dependence of K and P^+ is often ignored [28].

An elaborate account of the implication of this term can be found in [14]. Here, we are particularly interested in how sensitive the postupdate uncertainty P^+ is to uncertainties in estimates of K. To demonstrate this, Fig. 13 shows the fractional change in P^+ given a 10% deviation from the optimum value of K for different levels of x^- and for varying ratios between R and P^-, and between Σ_o and P^-, respectively. It is clear that the sensitivity of P^+ to suboptimality in the Kalman gain vanishes the larger x^- or Σ_o become. In other words, the larger the representativeness error, the less important it is how accurately model and observation uncertainties (i.e., $\mathbf{P}/\mathbf{R}$) are parameterized, especially if representativeness error is accounted for as part of the observation uncertainty (which is the common thing to do).

It should be noted, however, that the exact numbers shown in Fig. 13 are certainly not representing the exact behavior of the system used in this study; remember that we substitute a multivariate, nonlinear, state-variable-dependent observation operator with a scalar linear one. For a soil moisture DA system, the $x^{-2}\Sigma_o$ term in (8) would intuitively suggest that wetter states lead to higher analysis uncertainty. In reality, however, things are likely more complex because the observation operator is a nonlinear operator applied to x^-, and x^- is a state vector that contains a combination of different surface and root-zone soil

moisture and temperature-related variables. Notwithstanding, it is plausible that the general behavior observed in Fig. 13 still applies. That is, representativeness error can render the posterior uncertainty insensitive to small changes in the Kalman gain. This would at least partly explain why the significant differences between the observation uncertainties used in the DA_* and the $CTRL$ experiments do not lead to noteworthy differences in analysis skill.

VI. Conclusion

In this study, we assimilate SMAP T_b observations into NASA's CLSM using an EnKF with the goal of optimizing the uncertainty parameterization to achieve optimal filter performance. To account for the nonwhiteness of forecast and observation errors, T_b observations are assimilated on different timescales including: 1) anomalies (i.e., residuals from the mean seasonal cycle); 2) LF signal variations (i.e., interannual variations); and 3) HF signal variations (i.e., subseasonal variations). We assimilate T_b observations on each of these timescales separately as well as the LF and HF signal together, in each case optimizing the KF for the uncertainty of each assimilated signal component. As a benchmark, we assimilate T_b observations using a spatially constant observation error of 4 K, as is used for the generation of the operational SMAP L4 product.

To optimize the weights that the DA system puts on the observations, the *ratio* between the uncertainties of modeled and observed T_b is approximated using modeled (OL) and observed soil moisture uncertainties estimated using TCA. This approach is based on the premise that the optimal weight for assimilating T_b observations is likely very similar to the optimal weight for assimilating soil moisture retrievals. It also leverages SMAP soil moisture retrieval uncertainty estimates to account implicitly for representativeness error in the observation operator that our DA system uses to convert between soil moisture and T_b space. We discuss various caveats (e.g., the fact that using OL soil moisture uncertainty estimates will lead to systematically overestimated Kalman gains) and test whether their combined effect is small enough to still yield noteworthy skill improvements compared to the benchmark DA experiment.

All the experiments are evaluated using internal DA diagnostics and against both ground and satellite reference data. Assimilating SMAP T_b observations leads to significant improvements in both surface and root-zone soil moisture simulations of anomalies and LF signal variations. Simulations of HF surface soil moisture variations also benefit from the assimilation but to a smaller degree, and these improvements are only observed in the comparison against ground reference data.

Perhaps the most striking finding of this study is that the skill gain of our DA experiments that use optimized observation uncertainties differs, on all timescales, only marginally from that of the benchmark experiment that uses a spatially constant observation error of 4 K. In fact, changing the Kalman gain (within reasonable boundaries) does not seem to affect the "optimality" of the KF at all. We show, by analytical means, that one plausible explanation for this might be that the skill gain of a DA system is inherently restrained by representativeness errors. This is because they have the potential to render the postupdate uncertainty insensitive to small changes in the Kalman gain. Further evidence for this could be obtained by testing for consistency in the results when assimilating L2 soil moisture retrievals using the same TCA-based uncertainty tuning approach, but this is beyond the scope of this article.

One important source for representativeness error in observation operators is vegetation. Several studies have shown recently that shortcomings in the accounting for vegetation effects might be the most limiting factor in radiative transfer modeling [49], [82], [83]. Some of these shortcomings could be addressed by better exploiting both soil moisture and vegetation information contained in remotely sensed microwave signals in joint soil moisture and vegetation DA systems [84].

In conclusion, our results suggest that the focus of future research should shift from searching for more sophisticated uncertainty tuning approaches to improving observation operators that better bridge the gap between modeling systems and real-world observations. Such improvements may come from the physical modeling community [82], [83] but also be fostered by data-driven approaches [9], [27].

Acknowledgment

The authors would like to thank the editor and three anonymous reviewers for the time and effort they have put into providing constructive and thoughtful comments, which greatly benefited this article. The authors would also like to thank Gabrielle De Lannoy for valuable discussions.

References

[1] E. Han, W. T. Crow, T. Holmes, and J. Bolten, "Benchmarking a soil moisture data assimilation system for agricultural drought monitoring," *J. Hydrometeorol.*, vol. 15, no. 3, pp. 1117–1134, 2014.

[2] S. I. Seneviratne et al., "Investigating soil moisture–climate interactions in a changing climate: A review," *Earth-Sci. Rev.*, vol. 99, nos. 3/4, pp. 125–161, 2010.

[3] L. J. Renzullo et al., "Continental satellite soil moisture data assimilation improves root-zone moisture analysis for water resources assessment," *J. Hydrol.*, vol. 519, pp. 2747–2762, 2014.

[4] A. Gruber, W. Crow, W. Dorigo, and W. Wagner, "The potential of 2D Kalman filtering for soil moisture data assimilation," *Remote Sens. Environ.*, vol. 171, pp. 137–148, 2015.

[5] C. Albergel et al., "LDAS-monde sequential assimilation of satellite derived observations applied to the contiguous US: An ERA-5 driven reanalysis of the land surface variables," *Remote Sens.*, vol. 10, no. 10, 2018, Art. no. 1627.

[6] C. Draper and R. H. Reichle, "Assimilation of satellite soil moisture for improved atmospheric reanalyses," *Monthly Weather Rev.*, vol. 147, no. 6, pp. 2163–2188, 2019.

[7] H. Lievens, B. Martens, N. Verhoest, S. Hahn, R. Reichle, and D. G. Miralles, "Assimilation of global radar backscatter and radiometer brightness temperature observations to improve soil moisture and land evaporation estimates," *Remote Sens. Environ.*, vol. 189, pp. 194–210, 2017.

[8] J. Muñoz-Sabater et al., "Assimilation of SMOS brightness temperatures in the ECMWF integrated forecasting system," *Quart. J. Roy. Meteorol. Soc.*, vol. 145, no. 723, pp. 2524–2548, 2019.

[9] D. Rains, H. Lievens, G. J. De Lannoy, M. F. McCabe, R. A. de Jeu, and D. G. Miralles, "Sentinel-1 backscatter assimilation using support vector regression or the water cloud model at European soil moisture sites," *IEEE Geosci. Remote Sens. Lett.*, vol. 19, 2022, Art. no. 4013105.

[10] R. H. Reichle, S. Q. Zhang, Q. Liu, C. S. Draper, J. Kolassa, and R. Todling, "Assimilation of SMAP brightness temperature observations in the GEOS land–Atmosphere data assimilation system," *IEEE J. Sel. Topics Appl. Earth Observ. Remote Sens.*, vol. 14, pp. 10628–10643, 2021.

[11] G. J. De Lannoy and R. H. Reichle, "Assimilation of SMOS brightness temperatures or soil moisture retrievals into a land surface model," *Hydrol. Earth Syst. Sci.*, vol. 20, no. 12, pp. 4895–4911, 2016.

[12] L. Sun, S. Belair, M. L. Carrera, B. Bilodeau, and M. Dabboor, "Comparing assimilation of synthetic soil moisture versus C-band backscatter for hyper-resolution land surface modeling," *Water Resour. Res.*, vol. 57, no. 4, 2021, Art. no. e2020WR028921.

[13] S. Migliorini, "On the equivalence between radiance and retrieval assimilation," *Monthly Weather Rev.*, vol. 140, no. 1, pp. 258–265, 2012.

[14] P. J. Van Leeuwen, "Representation errors and retrievals in linear and nonlinear data assimilation," *Quart. J. Roy. Meteorol. Soc.*, vol. 141, no. 690, pp. 1612–1623, 2015.

[15] P. De Rosnay, M. Drusch, D. Vasiljevic, G. Balsamo, C. Albergel, and L. Isaksen, "A simplified extended Kalman filter for the global operational soil moisture analysis at ECMWF," *Quart. J. Roy. Meteorol. Soc.*, vol. 139, no. 674, pp. 1199–1213, 2013.

[16] R. Reichle et al., "Assessment of the SMAP level-4 surface and root-zone soil moisture product using in situ measurements," *J. Hydrometeorol.*, vol. 18, no. 10, pp. 2621–2645, 2017.

[17] R. H. Reichle, G. J. De Lannoy, B. A. Forman, C. S. Draper, and Q. Liu, "Connecting satellite observations with water cycle variables through land data assimilation: Examples using the nasa GEOS-5 LDAS," *Surv. Geophys.*, vol. 35, no. 3, pp. 577–606, 2014.

[18] W. Lahoz and G. De Lannoy, "Closing the gaps in our knowledge of the hydrological cycle over land: Conceptual problems," *Surv. Geophys.*, vol. 35, no. 3, pp. 623–660, 2014.

[19] G. J. De Lannoy and R. H. Reichle, "Global assimilation of multiangle and multipolarization SMOS brightness temperature observations into the GEOS-5 catchment land surface model for soil moisture estimation," *J. Hydrometeorol.*, vol. 17, no. 2, pp. 669–691, 2016.

[20] M. Durand and S. A. Margulis, "Correcting first-order errors in snow water equivalent estimates using a multifrequency, multiscale radiometric data assimilation scheme," *J. Geophys. Res.: Atmos.*, vol. 112, 2007, Art. no. D13121.

[21] R. H. Reichle, W. T. Crow, and C. L. Keppenne, "An adaptive ensemble Kalman filter for soil moisture data assimilation," *Water Resour. Res.*, vol. 44, no. 3, 2008, Art. no. W03423.

[22] G. J. De Lannoy, P. R. Houser, N. E. Verhoest, and V. R. Pauwels, "Adaptive soil moisture profile filtering for horizontal information propagation in the independent column-based CLM2.0," *J. Hydrometeorol.*, vol. 10, no. 3, pp. 766–779, 2009.

[23] G. Desroziers and S. Ivanov, "Diagnosis and adaptive tuning of observation-error parameters in a variational assimilation," *Quart. J. Roy. Meteorol. Soc.*, vol. 127, no. 574, pp. 1433–1452, 2001.

[24] G. Evensen, "The ensemble Kalman filter: Theoretical formulation and practical implementation," *Ocean Dyn.*, vol. 53, no. 4, pp. 343–367, 2003.

[25] C. Anderson et al., "Validation of backscatter measurements from the advanced scatterometer on MetOp-A," *J. Atmos. Ocean. Technol.*, vol. 29, no. 1, pp. 77–88, 2011.

[26] J. Peng et al., "Soil moisture active/passive (SMAP) l-band microwave radiometer post-launch calibration upgrade," *IEEE J. Sel. Topics Appl. Earth Observ. Remote Sens.*, vol. 12, no. 6, pp. 1647–1657, Jun. 2019.

[27] N. Rodríguez-Fernández et al., "SMOS neural network soil moisture data assimilation in a land surface model and atmospheric impact," *Remote Sens.*, vol. 11, no. 11, 2019, Art. no. 1334.

[28] T. Janjić et al., "On the representation error in data assimilation," *Quart. J. Roy. Meteorol. Soc.*, vol. 144, no. 713, pp. 1257–1278, 2018.

[29] R. Mehra, "On the identification of variances and adaptive Kalman filtering," *IEEE Trans. Autom. Control*, vol. AC-15, no. 2, pp. 175–184, Apr. 1970.

[30] D. P. Dee, "On-line estimation of error covariance parameters for atmospheric data assimilation," *Monthly Weather Rev.*, vol. 123, no. 4, pp. 1128–1145, 1995.

[31] G. Desroziers, L. Berre, B. Chapnik, and P. Poli, "Diagnosis of observation, background and analysis-error statistics in observation space," *Quart. J. Roy. Meteorol. Soc.*, vol. 131, no. 613, pp. 3385–3396, 2005.

[32] W. Crow and M. T. Yilmaz, "The auto-tuned land data assimilation system (ATLAS)," *Water Resour. Res.*, vol. 50, no. 1, pp. 371–385, 2014.

[33] P. Tandeo et al., "A review of innovation-based methods to jointly estimate model and observation error covariance matrices in ensemble data assimilation," *Monthly Weather Rev.*, vol. 148, no. 10, pp. 3973–3994, 2020.

[34] W. Crow and R. Reichle, "Comparison of adaptive filtering techniques for land surface data assimilation," *Water Resour. Res.*, vol. 44, no. 8, 2008, Art. no. W08423.

[35] A. Gruber, G. D. Lannoy, and W. Crow, "A Monte Carlo based adaptive Kalman filtering framework for soil moisture data assimilation," *Remote Sens. Environ.*, vol. 228, pp. 105–114, 2019.

[36] A. Gelb, *Applied Optimal Estimation*. Cambridge, MA, USA: MIT Press, 1974.

[37] W. Crow and M. Van den Berg, "An improved approach for estimating observation and model error parameters in soil moisture data assimilation," *Water Resour. Res.*, vol. 46, no. 12, 2010, Art. no. W12519.

[38] C. Draper, R. Reichle, G. De Lannoy, and Q. Liu, "Assimilation of passive and active microwave soil moisture retrievals," *Geophys. Res. Lett.*, vol. 39, no. 4, 2012, Art. no. 5555.

[39] R. Reichle et al., "Global assessment of the SMAP level-4 surface and root-zone soil moisture product using assimilation diagnostics," *J. Hydrometeorol.*, vol. 18, no. 12, pp. 3217–3237, 2017.

[40] E. Seo, M.-I. Lee, and R. H. Reichle, "Assimilation of SMAP and ASCAT soil moisture retrievals into the JULES land surface model using the local ensemble transform Kalman filter," *Remote Sens. Environ.*, vol. 253, 2021, Art. no. 112222.

[41] A. Stoffelen, "Toward the true near-surface wind speed: Error modeling and calibration using triple collocation," *J. Geophys. Res.*, vol. 103, no. C4, pp. 7755–7766, 1998.

[42] A. Gruber, W. Crow, and W. Dorigo, "Assimilation of spatially sparse in situ soil moisture networks into a continuous model domain," *Water Resour. Res.*, vol. 54, no. 2, pp. 1353–1367, 2018.

[43] K. Wu, H. Shu, L. Nie, and Z. Jiao, "Triple collocation-based estimation of spatially correlated observation error covariance in remote sensing soil moisture data assimilation," *J. Appl. Remote Sens.*, vol. 12, no. 1, 2018, Art. no. 016039.

[44] A. Gruber, C.-H. Su, S. Zwieback, W. Crow, W. Dorigo, and W. Wagner, "Recent advances in (soil moisture) triple collocation analysis," *Int. J. Appl. Earth Observ. Geoinf.*, vol. 45, pp. 200–211, 2016.

[45] S. Zwieback, W. Dorigo, and W. Wagner, "Temporal error variability of coarse scale soil moisture products-case study in Central Spain," in *Proc. IEEE Int. Geosci. Remote Sens. Symp.*, 2012, pp. 722–725.

[46] K. Wu, D. Ryu, L. Nie, and H. Shu, "Time-variant error characterization of SMAP and ASCAT soil moisture using triple collocation analysis," *Remote Sens. Environ.*, vol. 256, 2021, Art. no. 112324.

[47] C. Draper and R. Reichle, "The impact of near-surface soil moisture assimilation at subseasonal, seasonal, and inter-annual timescales," *Hydrol. Earth Syst. Sci.*, vol. 19, no. 12, 2015, Art. no. 4831.

[48] C. Massari et al., "A review of irrigation information retrievals from space and their utility for users," *Remote Sens.*, vol. 13, no. 20, 2021, Art. no. 4112.

[49] S. Zwieback et al., "Estimating time-dependent vegetation biases in the SMAP soil moisture product," *Hydrol. Earth Syst. Sci.*, vol. 22, no. 8, pp. 4473–4489, 2018.

[50] C.-H. Su, D. Ryu, W. T. Crow, and A. W. Western, "Stand-alone error characterisation of microwave satellite soil moisture using a Fourier method," *Remote Sens. Environ.*, vol. 154, pp. 115–126, 2014.

[51] R. Gelaro et al., "The modern-era retrospective analysis for research and applications, version 2 (MERRA-2)," *J. Climate*, vol. 30, no. 14, pp. 5419–5454, 2017.

[52] S. Chan, E. G. Njoku, and A. Colliander, "SMAP L1C radiometer half-orbit 36 km ease-grid brightness temperatures, Version 5," NASA National Snow and Ice Data Center Distributed Active Archive Center, Boulder, CO, USA, Tech. Rep. SPL1CTB, 2020.

[53] P. O'Neill, S. Chan, E. Njoku, T. Jackson, and R. Blindish, "SMAP L2 radiometer half-orbit 36 km EASE-grid soil moisture, Version 5," NASA National Snow and ice Data Center Distributed Active Archive Center, Boulder, CO, USA, 2018.

[54] W. Wagner, G. Lemoine, and H. Rott, "A method for estimating soil moisture from ERS scatterometer and soil data," *Remote Sens. Environ.*, vol. 70, no. 2, pp. 191–207, 1999.

[55] V. Naeimi, K. Scipal, Z. Bartalis, S. Hasenauer, and W. Wagner, "An improved soil moisture retrieval algorithm for ERS and METOP scatterometer observations," *IEEE Trans. Geosci. Remote Sens.*, vol. 47, no. 7, pp. 1999–2013, Jul. 2009.

[56] G. L. Schaefer, M. H. Cosh, and T. J. Jackson, "The USDA natural resources conservation service soil climate analysis network (SCAN)," *J. Atmos. Ocean. Technol.*, vol. 24, no. 12, pp. 2073–2077, 2007.

[57] J. Bell et al., "US climate reference network soil moisture and temperature observations," *J. Hydrometeorol.*, vol. 14, no. 3, pp. 977–988, 2013.

[58] W. Dorigo et al., "Global automated quality control of in situ soil moisture data from the international soil moisture network," *Vadose Zone J.*, vol. 12, no. 3, pp. 1–21, 2013.

[59] W. Dorigo et al., "The international soil moisture network: Serving Earth system science for over a decade," *Hydrol. Earth Syst. Sci.*, vol. 25, no. 11, pp. 5749–5804, 2021.
[60] M. J. Brodzik, B. Billingsley, T. Haran, B. Raup, and M. H. Savoie, "EASE-Grid 2.0: Incremental but significant improvements for earth-gridded data sets," *ISPRS Int. J. Geo-Inf.*, vol. 1, no. 1, pp. 32–45, 2012.
[61] R. D. Koster, M. J. Suarez, A. Ducharne, M. Stieglitz, and P. Kumar, "A catchment-based approach to modeling land surface processes in a general circulation model: 1. Model structure," *J. Geophys. Res.: Atmos.*, vol. 105, no. D20, pp. 24809–24822, 2000.
[62] G. J. De Lannoy, R. H. Reichle, and V. R. Pauwels, "Global calibration of the GEOS-5 l-band microwave radiative transfer model over non-frozen land using SMOS observations," *J. Hydrometeorol.*, vol. 14, no. 3, pp. 765–785, 2013.
[63] R. H. Reichle et al., "Version 4 of the SMAP level-4 soil moisture algorithm and data product," *J. Adv. Model. Earth Syst.*, vol. 11, no. 10, pp. 3106–3130, Oct. 2019.
[64] D. P. Dee and A. M. Da Silva, "Data assimilation in the presence of forecast bias," *Quart. J. Roy. Meteorol. Soc.*, vol. 124, no. 545, pp. 269–295, 1998.
[65] W. T. Crow, R. D. Koster, R. H. Reichle, and H. O. Sharif, "Relevance of time-varying and time-invariant retrieval error sources on the utility of spaceborne soil moisture products," *Geophys. Res. Lett.*, vol. 32, no. 24, 2005, Art. no. L24405.
[66] R. H. Reichle et al., "Recent advances in land data assimilation at the NASA global modeling and assimilation office," in *Data Assimilation for Atmospheric, Oceanic and Hydrologic Applications*. New York, NY, USA: Springer, 2009, pp. 407–428.
[67] D. P. Dee, "Bias and data assimilation," *Quart. J. Roy. Meteorol. Soc.*, vol. 131, no. 613, pp. 3323–3343, 2005.
[68] M. Drusch, E. Wood, and H. Gao, "Observation operators for the direct assimilation of TRMM microwave imager retrieved soil moisture," *Geophys. Res. Lett.*, vol. 32, no. 15, 2005, Art. no. L15403.
[69] S. V. Kumar, R. H. Reichle, K. W. Harrison, C. D. Peters-Lidard, S. Yatheendradas, and J. A. Santanello, "A comparison of methods for a priori bias correction in soil moisture data assimilation," *Water Resour. Res.*, vol. 48, no. 3, 2012, Art. no. W03515.
[70] M. T. Yilmaz and W. T. Crow, "The optimality of potential rescaling approaches in land data assimilation," *J. Hydrometeorol.*, vol. 14, no. 2, pp. 650–660, 2013.
[71] A. Gruber et al., "Validation practices for satellite soil moisture retrievals: What are (the) errors?," *Remote Sens. Environ.*, vol. 244, 2020, Art. no. 111806.
[72] K. Scipal, T. Holmes, R. de Jeu, V. Naeimi, and W. Wagner, "A possible solution for the problem of estimating the error structure of global soil moisture data sets," *Geophys. Res. Lett.*, vol. 35, no. 24, 2008, Art. no. L24403.
[73] A. Gruber, T. Scanlon, R. van der Schalie, W. Wagner, and W. Dorigo, "Evolution of the ESA CCI soil moisture climate data records and their underlying merging methodology," *Earth Syst. Sci. Data*, vol. 11, no. 2, pp. 717–739, 2019.
[74] K. A. McColl, A. Roy, C. Derksen, A. G. Konings, S. H. Alemohammed, and D. Entekhabi, "Triple collocation for binary and categorical variables: Application to validating landscape freeze/thaw retrievals," *Remote Sens. Environ.*, vol. 176, pp. 31–42, 2016.
[75] C. Draper, R. Reichle, R. de Jeu, V. Naeimi, R. Parinussa, and W. Wagner, "Estimating root mean square errors in remotely sensed soil moisture over continental scale domains," *Remote Sens. Environ.*, vol. 137, pp. 288–298, 2013.
[76] W. Dorigo et al., "ESA CCI soil moisture for improved earth system understanding: State-of-the Art and future directions," *Remote Sens. Environ.*, vol. 203, pp. 185–215, 2017.
[77] A. Al-Yaari et al., "Global-scale comparison of passive (SMOS) and active (ASCAT) satellite based microwave soil moisture retrievals with soil moisture simulations (MERRA-Land)," *Remote Sens. Environ.*, vol. 152, pp. 614–626, 2014.
[78] J. Dong, W. Crow, R. Reichle, Q. Liu, F. Lei, and M. H. Cosh, "A global assessment of added value in the SMAP level 4 soil moisture product relative to its baseline land surface model," *Geophys. Res. Lett.*, vol. 46, no. 12, pp. 6604–6613, 2019.
[79] R. H. Reichle et al., "The contributions of gauge-based precipitation and SMAP brightness temperature observations to the skill of the SMAP level-4 soil moisture product," *J. Hydrometeorol.*, vol. 22, no. 2, pp. 405–424, 2021.
[80] F. Zaussinger, W. Dorigo, A. Gruber, A. Tarpanelli, P. Filippucci, and L. Brocca, "Estimating irrigation water use over the contiguous United States by combining satellite and reanalysis soil moisture data," *Hydrol. Earth Syst. Sci.*, vol. 23, no. 2, pp. 897–923, 2019.
[81] C. Draper and R. Reichle, "Observation error specification for near-surface soil moisture assimilation: Does it matter?," in *Proc. Amer. Meteorol. Soc. Annu. Meeting*, 2018, Art. no. GSFC-E-DAA-TN51745.
[82] J.-P. Wigneron et al., "Modelling the passive microwave signature from land surfaces: A review of recent results and application to the L-band SMOS & SMAP soil moisture retrieval algorithms," *Remote Sens. Environ.*, vol. 192, pp. 238–262, 2017.
[83] R. Quast, C. Albergel, J.-C. Calvet, and W. Wagner, "A generic first-order radiative transfer modelling approach for the inversion of soil and vegetation parameters from scatterometer observations," *Remote Sens.*, vol. 11, no. 3, 2019, Art. no. 285.
[84] C. Albergel et al., "Sequential assimilation of satellite-derived vegetation and soil moisture products using SURFEX_v8.0: LDAS-monde assessment over the Euro-Mediterranean area," *Geosci. Model Develop.*, vol. 10, no. 10, pp. 3889–3912, 2017.

Alexander Gruber received the M.Sc. degree in geodesy and geophysics and the Ph.D. degree in technical sciences from the Vienna University of Technology, Vienna, Austria, in 2013 and 2016, respectively.

He is currently a Postdoctoral Researcher with the Climate and Environmental Remote Sensing Research Group, Department of Geodesy and Geoinformation, Vienna University of Technology. His research interests include land surface remote sensing, data assimilation, uncertainty characterization, and water and carbon cycle interactions.

Rolf H. Reichle received the M.S. degree (Diplom) in physics from the University of Heidelberg, Heidelberg, Germany, in 1996, and the Ph.D. degree in environmental engineering from the Massachusetts Institute of Technology, Cambridge, MA, USA, in 2000.

He is currently a Research Physical Scientist with the Global Modeling and Assimilation Office, NASA Goddard Space Flight Center, Greenbelt, MD, USA. His research interests include land data assimilation, satellite-based remote sensing, and applications related to land–atmosphere interactions, weather prediction, and seasonal climate forecasting.